



Published in final edited form as:

Nature. 2021 February ; 590(7846): 473–479. doi:10.1038/s41586-020-03116-4.

Gut-licensed IFN γ + NK cells drive LAMP1+TRAIL+ anti-inflammatory astrocytes

Liliana M. Sanmarco^{1,9}, Michael A. Wheeler^{1,2,9}, Cristina Gutiérrez-Vázquez¹, Carolina Manganeli Polonio¹, Mathias Linnerbauer¹, Felipe A. Pinho-Ribeiro³, Zhaorong Li^{1,2}, Federico Giovannoni¹, Katelyn V. Batterman⁴, Giulia Scalisi¹, Stephanie E. J. Zandee^{5,6}, Evelyn S. Heck¹, Moneera Alsuwailm^{1,7}, Douglas L. Rosene⁴, Burkhard Becher⁸, Isaac M. Chiu³, Alexandre Prat^{5,6}, Francisco J. Quintana^{1,2}

¹Ann Romney Center for Neurologic Diseases, Brigham and Women's Hospital, Harvard Medical School, Boston, MA, USA. ²Broad Institute of MIT and Harvard, Cambridge, MA, USA.

³Department of Immunology, Harvard Medical School, Boston, MA, USA. ⁴Department of Anatomy and Neurobiology, Boston University School of Medicine, Boston, MA, USA.

⁵Neuroimmunology Unit, Centre de Recherche du CHUM, Montréal, Quebec, Canada.

⁶Department of Neuroscience, Faculty of Medicine, Université de Montréal, Montréal, Quebec, Canada. ⁷Center of Excellence for Biomedicine, Joint Centers of Excellence Program, King Abdulaziz City for Science and Technology (KACST), Riyadh, Saudi Arabia. ⁸Institute of Experimental Immunology, University of Zurich, Zurich, Switzerland.

Abstract

Astrocytes are glial cells that are abundant in the central nervous system (CNS) and that have important homeostatic and disease-promoting functions¹. However, little is known about the homeostatic anti-inflammatory activities of astrocytes and their regulation. Here, using high-throughput flow cytometry screening, single-cell RNA sequencing and CRISPR–Cas9-based cell-specific in vivo genetic perturbations in mice, we identify a subset of astrocytes that expresses the lysosomal protein LAMP1² and the death receptor ligand TRAIL³. LAMP1⁺TRAIL⁺ astrocytes limit inflammation in the CNS by inducing T cell apoptosis through TRAIL–DR5 signalling. In homeostatic conditions, the expression of TRAIL in astrocytes is driven by interferon- γ (IFN γ)

Reprints and permissions information is available at <http://www.nature.com/reprints>.

Correspondence and requests for materials should be addressed to F.J.Q. fquintana@rics.bwh.harvard.edu.

⁹These authors contributed equally: Liliana M. Sanmarco, Michael A. Wheeler.

Author contributions L.M.S. and M.A.W. performed most in vivo, in vitro, FACS and genomics experiments. C.G.-V., C.M.P., M.L., F.G., G.S., E.S.H. and M.A. assisted with in vivo, in vitro, FACS and genomics experiments. F.A.P.-R. assisted with isolation and immunostaining of the meninges. L.M.S., M.A.W. and Z.L. performed bioinformatic analyses. K.V.B. performed RNAscope studies with L.M.S. and M.A.W. S.E.J.Z., D.L.R., B.B., I.M.C. and A.P. provided unique reagents and/or discussed and interpreted findings. L.M.S., M.A.W. and F.J.Q. wrote the manuscript with input from all co-authors. F.J.Q. designed and supervised the study and edited the manuscript.

Competing interests The authors declare no competing interests.

Supplementary information The online version contains supplementary material available at <https://doi.org/10.1038/s41586-020-03116-4>.

Peer review information *Nature* thanks Peter Calabresi, Hartmut Wekerle and the other, anonymous, reviewer(s) for their contribution to the peer review of this work.

Publisher's note Springer Nature remains neutral with regard to jurisdictional claims in published maps and institutional affiliations.

produced by meningeal natural killer (NK) cells, in which IFN γ expression is modulated by the gut microbiome. TRAIL expression in astrocytes is repressed by molecules produced by T cells and microglia in the context of inflammation. Altogether, we show that LAMP1⁺TRAIL⁺ astrocytes limit CNS inflammation by inducing T cell apoptosis, and that this astrocyte subset is maintained by meningeal IFN γ ⁺ NK cells that are licensed by the microbiome.

Astrocytes are abundant cells in the CNS that perform important functions in development and homeostasis associated with neuron metabolism^{4,5}, regulation of neural activity⁶, production of synaptogenic factors⁷, and control of the glia limitans⁸ and the blood–brain barrier⁹. These homeostatic mechanisms are central to CNS physiology, and their dysregulation contributes to the pathogenesis of neurological diseases⁸. In addition, in the context of neurological disorders, astrocytes acquire functions that promote and amplify CNS pathology, such as neurotoxic activity, and the ability to activate microglia and recruit peripheral pro-inflammatory cells¹⁰⁻¹³. This breadth of astrocyte functions reflects the existence of diverse—and potentially plastic—astrocyte subsets or activation states that are associated with homeostatic and pathogenic activities¹⁴⁻¹⁶. Although multiple pathogenic functions have been defined for astrocytes in the context of CNS inflammation¹, less is known about the homeostatic anti-inflammatory activities of astrocytes and their regulation.

T cells recruited to the inflamed CNS can modulate astrocyte responses¹⁶⁻¹⁸, but astrocytes can potentially respond to molecules produced by other peripheral immune cells in the meninges during homeostasis¹⁹. In addition, some microbial metabolites have been shown to reach the CNS and act directly on astrocytes²⁰ and microglia²¹⁻²⁴ to modulate their phenotype and function. Here we describe a subset of astrocytes that is driven by IFN γ produced by meningeal NK cells, and show that IFN γ expression in these NK cells is modulated by the commensal flora. This subpopulation of astrocytes limits inflammation in the CNS by inducing TRAIL-dependent apoptosis in pro-inflammatory T cells.

Identification of LAMP1⁺ astrocytes

To identify novel subsets of astrocytes, we used flow cytometry to assess the binding of 266 antibodies to mouse astrocytes expressing enhanced green fluorescent protein (EGFP) under the control of the *Aldh1l1* promoter (*Aldh1l1*^{EGFP} mice) (Fig. 1a-c, Extended Data Fig. 1, Supplementary Table 1). Approximately 60 antibodies showed higher reactivity with *Aldh1l1*^{EGFP} astrocytes than with *Aldh1l1*⁻ cells (Fig. 1b, c, Extended Data Fig. 1, Supplementary Table 1). We then analysed the expression of the top 15 surface markers in *Aldh1l1*^{creERT2tdTomato} spinal cord astrocytes isolated from naive mice or from mice 16 and 27 days (peak and recovery, respectively) after the induction of experimental autoimmune encephalomyelitis (EAE) by immunization with MOG₃₅₋₅₅ peptide. The most abundant marker expressed by spinal cord astrocytes was lysosomal-associated membrane protein 1 (LAMP1; also known as CD107a)², which was upregulated during EAE in spinal cord astrocytes, but not in cerebellar, cortical or parenchymal (subcortical) astrocytes (Fig. 1d-g, Extended Data Fig. 2a-c).

LAMP1⁺ astrocytes express TRAIL

LAMP1 is a lysosomal protein that is detectable in the cell membrane and is linked to cytotoxic activity². To investigate its role during EAE, we inactivated *Lamp1* in astrocytes using a lentivirus that co-expresses *Gfap*-driven CRISPR–Cas9 and either a *Lamp1*-targeting or a non-targeting single-guide RNA (sgRNA)²⁵ (Extended Data Fig. 3a-c). Inactivation of *Lamp1* in astrocytes worsened EAE, increased the number of IFN γ - and/or interleukin 17 (IL-17)-expressing CD4⁺ T cells in the CNS and activated astrocyte pro-inflammatory pathways, but did not affect CD8⁺ T cells, FOXP3⁺ T_{reg} cells (that is, CD4⁺CD25⁺ T cells), pro-inflammatory monocytes, CNS-resident cells or peripheral T cells (Fig. 2a-d, Extended Data Fig. 3d-f, Supplementary Table 2).

On the basis of the role of T cell apoptosis in limiting the development of EAE²⁶⁻²⁸, we investigated whether LAMP1⁺ astrocytes induced T cell death. In mice treated with an sgRNA against *Lamp1* we detected a decreased activation of pro-apoptotic caspase-3 in CNS-recruited CD4⁺ T cells (Fig. 2e), but not in CD11b⁺ cells (Extended Data Fig. 3g). To identify apoptosis-inducing molecules in LAMP1⁺ astrocytes, we analysed antibody-labelled LAMP1⁺ *Aldh11^{creERT2tdTomato}* astrocytes from naive or peak EAE mice by single-cell RNA sequencing (scRNA-seq) (Fig. 2f, Extended Data Fig. 3h-j, Supplementary Table 3). In LAMP1⁺ astrocytes we detected the expression of *Tnfsf10* (Fig. 2f)—which encodes the pro-apoptotic death receptor ligand TRAIL³—but not that of genes encoding other pro-apoptotic molecules (Extended Data Fig. 3j). Inactivation of *Lamp1* in astrocytes reduced the surface expression of TRAIL in vivo, suggesting that LAMP1 controls the trafficking of TRAIL to the cell membrane (Extended Data Fig. 3k). Moreover, *Tnfsf10*-expressing LAMP1⁺ astrocytes were decreased in mice with EAE (Fig. 2g).

TRAIL⁺ astrocytes limit EAE development

TRAIL and other members of the tumour necrosis factor (TNF) family regulate the immune response by inducing apoptosis³, suggesting that LAMP1⁺TRAIL⁺ astrocytes might limit CNS inflammation by promoting pathogenic T cell apoptosis. To test this hypothesis, we inactivated *Tnfsf10* in mouse astrocytes using *Gfap*-driven CRISPR–Cas9 lentivirus, and induced EAE by immunization with MOG₃₅₋₅₅. Inactivation of *Tnfsf10* in astrocytes worsened EAE and increased the numbers of T cells in the CNS while reducing caspase-3 activation in CNS-recruited CD4⁺ T cells, but did not affect CNS-resident cells, levels of apoptosis in CD11b⁺ cells or peripheral CD4⁺ T cells, or the recall responses of peripheral CD4⁺ T cells (Fig. 3a-c, Extended Data Fig. 4a-e). Consistent with these findings, knockdown of *Tnfsf10* activated pro-inflammatory pathways in astrocytes (Fig. 3d, Supplementary Table 4).

To investigate the regulation of TRAIL expression, we analysed antibody-labelled LAMP1⁺TRAIL⁺ *Aldh11^{creERT2tdTomato}* astrocytes from naive or peak EAE mice by scRNA-seq (Fig. 3e, Extended Data Fig. 4f-h, Supplementary Table 5). We identified a cluster of LAMP1⁺TRAIL⁺ astrocytes associated with naive mice, which was characterized by pro-apoptotic TRAIL signalling (Fig. 3e-g) and which contained a transcriptional signature associated with IFN γ signalling (Fig. 3h). We reanalysed a previously published

scRNA-seq dataset¹⁶ of astrocytes from mice with EAE and patients with multiple sclerosis (MS) and identified a similar population of astrocytes characterized by IFN γ and TRAIL signalling, which decreased by 37% and 84% during EAE and MS, respectively (Extended Data Fig. 5a-e). The same subset of astrocytes was identified when scRNA-seq studies were analysed at higher read depth (Extended Data Fig. 5f, Supplementary Table 6). Of note, naive LAMP1⁺TRAIL⁺ astrocytes were comparable in abundance to astrocytes driven by MAFG expression—which have previously been linked to EAE pathogenesis¹⁶—but were outnumbered by these pathogenic astrocytes during EAE (Extended Data Fig. 5c).

IFN γ drives TRAIL expression in astrocytes

Cytokines and other molecules produced by T cells and microglia control astrocyte responses^{15-17,22}. Treatment with IFN γ increased the expression of *Tnfsf10* in primary mouse astrocytes (and also in microglia and neurons) in culture, and induced the recruitment of phosphorylated STAT1 (pSTAT1) to the *Tnfsf10* promoter (Fig. 4a-c, Extended Data Fig. 6a, b). Treatment with IFN β induced some expression of *Tnfsf10*, and treatment with IFN γ also induced some expression of *FasI* and *Gzmb* (Fig. 4a, Extended Data Fig. 6c). However, IFN γ -induced expression of *Tnfsf10* in astrocytes was suppressed by granulocyte-macrophage colony-stimulating factor (GM-CSF), TNF, IL-1 α and complement component 1q (C1q) (Fig. 4d)—pro-inflammatory cytokines produced by T cells and microglia that induce disease-promoting responses in astrocytes during EAE and in patients with MS^{15,16,29}. Consistent with this, astrocytes deficient in TNF or GM-CSF signalling expressed less *Tnfsf10* during EAE (Extended Data Fig. 6d). Conversely, EAE mice lacking IFN γ receptor 1 (*Ifngr1*^{-/-}) exhibited fewer LAMP1⁺TRAIL⁺ astrocytes, concomitant with an increase in the number of CNS-recruited effector T cells and lower levels of T cell apoptosis in the CNS (Fig. 4e, Extended Data Fig. 6e-g). EAE was also worsened, in agreement with previous studies³⁰.

Inactivation of *Ifngr1*, *Ifngr2* and *Stat1* in mouse astrocytes using lentivirus-delivered *Gfap*-driven CRISPR-Cas9 and targeting sgRNAs (Extended Data Fig. 7a, b) worsened EAE, decreased TRAIL expression and increased the number of CNS-recruited T cells while reducing the levels of T cell apoptosis in the CNS (Fig. 4f-i). Astrocytes from knockdown mice showed an activation of pro-inflammatory pathways, and a decrease in IFN γ signalling and in the expression of *Cxcl10* (but not that of other chemokines or chemokine receptors) (Fig. 4j, k, Extended Data Fig. 7c, d, Supplementary Table 7). Likewise, microglia isolated after astrocyte-specific inactivation of IFN γ signalling exhibited pro-inflammatory transcriptional signatures, probably reflecting the increase in pro-inflammatory T cells in the CNS; CNS-recruited pro-inflammatory monocytes and peripheral T cells were unaffected (Extended Data Fig. 8a-h).

We found that astrocytes that were pretreated with IFN γ induced TRAIL-dependent apoptosis when cultured with CD4⁺ T cells (Fig. 4l, Extended Data Fig. 9a, b). An analysis of CD4⁺ T cells from EAE mice and CD4⁺ T cells that were polarized in vitro revealed that IL-17⁺CD4⁺ T cells express higher levels of death receptor 5 (DR5) (Fig. 4m, Extended Data Fig. 9c), which transduces TRAIL pro-apoptotic signals³¹. We detected more T cell apoptosis in DR5⁺CD4⁺ T cells (derived from peak EAE mice) cultured with IFN γ -pre-

treated astrocytes than in DR5⁻CD4⁺ T cells (Fig. 4n). Collectively, these data show that IFN γ -driven TRAIL⁺ astrocytes limit CNS inflammation by inducing T cell apoptosis through TRAIL–DR5 signalling, and that TRAIL expression in astrocytes is repressed by pro-inflammatory cytokines produced during EAE and MS.

Meningeal NK cells drive TRAIL expression

We detected TRAIL⁺ astrocytes located close to the meninges and IFN γ ⁺ cells in naive mice and samples from healthy individuals by immunostaining and in situ hybridization (Fig. 5a–d, Extended Data Fig. 9d–g). Although several cell types can produce IFN γ —including T cells, NK1.1⁺CD200R⁻ NK cells and NK1.1⁺CD200R⁺ type 1 innate lymphoid cells^{32,33}—we identified NK cells as the most abundant IFN γ producers in the meninges of naive mice and healthy individuals (using flow cytometry, reporter mice and immunostaining; Fig. 5e, f).

To assess the effects of IFN γ produced by NK cells on TRAIL⁺ astrocytes, we depleted NK1.1⁺ cells using an anti-NK1.1 monoclonal antibody (Fig. 5g, Extended Data Fig. 9h–j). Treatment with anti-NK1.1 decreased the number of TRAIL⁺ astrocytes (Fig. 5g), suggesting that NK1.1⁺-cell-derived IFN γ promotes TRAIL expression in astrocytes. In line with this, co-culturing astrocytes with IFN γ ⁺ NK cells—but not IFN γ ⁻ NK cells—led to an upregulation of TRAIL levels in astrocytes (Fig. 5h).

In agreement with the suppression of *Tnfrsf10* expression in astrocytes by pro-inflammatory cytokines (Fig. 4d, Extended Data Fig. 6d), TRAIL⁺ astrocytes were reduced in EAE and MS (Fig. 5a, b, d), and CD4⁺ T cells—not NK cells—were the most abundant IFN γ -producing cells in the CNS during EAE (Fig. 5i). Collectively, these findings suggest that meningeal IFN γ ⁺ NK cells promote TRAIL expression in astrocytes in homeostasis, but that pro-inflammatory cytokines limit TRAIL expression during EAE.

Gut-licensed IFN γ ⁺ NK cells induce TRAIL

The intestinal microbiome induces IFN γ expression in NK cells^{34,35}, suggesting that it may indirectly control the expression of TRAIL in astrocytes. Indeed, we detected fewer LAMP1⁺TRAIL⁺ astrocytes in germ-free mice than in specific-pathogen free (SPF) mice; total astrocyte numbers were similar (Fig. 6a, Extended Data Fig. 10a). Germ-free mice had fewer meningeal IFN γ ⁺ NK cells than SPF mice, but similar numbers of total meningeal NK cells (Fig. 6b, c), and fewer IFN γ ⁺NK1.1⁺CD200R⁻ NK cells and IFN γ ⁺CD4⁺ T cells in the intestinal lamina propria and spleen (Extended Data Fig. 10b–d). We then adoptively transferred NK1.1⁺ cells from germ-free wild-type, SPF wild-type or SPF *Ifng*^{-/-} mice into germ-free wild-type recipients (Fig. 6d). We detected more meningeal IFN γ ⁺NK1.1⁺ cells in recipients of SPF wild-type NK1.1⁺ cells than in either of the other two groups of recipients; total NK1.1⁺ cell numbers were similar (Fig. 6e, Extended Data Fig. 10d). In support of the idea that microbiome-induced IFN γ ⁺ production by NK cells has a role in the control of TRAIL expression in astrocytes, we detected more LAMP1⁺TRAIL⁺ astrocytes in recipients of SPF wild-type NK1.1⁺ cells than in recipients of germ-free wild-type or SPF *Ifng*^{-/-} NK1.1⁺ cells (Fig. 6f).

To study the control of IFN γ ⁺ NK cells and TRAIL⁺ astrocytes by the microbiome, we performed antibiotic depletion of the microbiota (ABX) and faecal microbiota transfer (FMT) studies in SPF *Irf1*^{EYFP} mice (Extended Data Fig. 10e). We detected fewer IFN γ ⁺ NK cells, but similar total numbers of NK cells, in the meninges, spleen and lamina propria of ABX-treated relative to vehicle- or ABX + FMT-treated mice (Fig. 6g, Extended Data Fig. 10f-h). The number of TRAIL⁺ astrocytes was also reduced in ABX-treated mice (Fig. 6g).

Finally, we evaluated the migration of NK cells using *CAG*^{Kaede} mice, which ubiquitously express a photoconvertible fluorescent protein³⁶. After photoconversion in the small intestine, photoconverted NK cells were detected in the meninges, but not in the CNS parenchyma (Fig. 6h-k, Extended Data Fig. 10i, j). ABX treatment reduced the expression of *Irf1* in photoconverted NK cells, but the splenic recruitment of NK cells was unaffected (Fig. 6k). Together, these data suggest that the gut microbiome licenses IFN γ expression in NK cells, which localize to the meninges to promote TRAIL expression in astrocytes.

Discussion

Single-cell analyses have identified several different populations and activation states of astrocytes that are associated with CNS development, homeostasis and disease^{4,14-16,20,22,25,37}. Here we report that TRAIL⁺ astrocytes, which are driven by the expression of IFN γ , limit inflammation in the CNS by inducing apoptosis in effector T cells. IFN γ produced by meningeal NK cells drives the expression of TRAIL in astrocytes, but IFN γ ⁺ NK cells do not infiltrate the CNS parenchyma in naive mice. Similarly, meningeal IFN γ ⁺ T cells influence mouse behaviour without infiltrating the CNS parenchyma³³. Molecules that are smaller than 40 kDa in the subarachnoid cerebrospinal fluid—which contains IFN γ in homeostatic conditions³⁸—are able to reach the perivascular endfeet of astrocytes. As most astrocytes contact blood vessels through endfeet extensions³⁹, these findings suggest that IFN γ produced by meningeal NK cells interacts with receptors in astrocytic endfeet to modulate TRAIL expression and other homeostatic functions. In homeostatic conditions, IFN γ might also drive TRAIL-dependent anti-inflammatory mechanisms in other cell types, such as neurons and microglia. Together with the previously documented effects of meningeal IFN γ on mouse behaviour³³ and learning⁴⁰, these findings highlight the physiological roles of IFN γ in homeostasis in the CNS.

IFN γ ⁺ NK cells drive the homeostatic expression of TRAIL in astrocytes. NK cells exhibit anti-inflammatory functions that are linked to decreased disease severity in patients with MS⁴¹, and modulators of IL-2 signalling normalize NK cell function in patients with MS⁴². As IL-2 drives the expression of IFN γ in NK cells⁴³, IL-2 might indirectly boost the IFN γ -driven immunoregulatory activities of astrocytes. Conversely, pathogens induce long-term changes in the phenotype and homing of NK cells⁴⁴. Thus, it is conceivable that viral and bacterial infections associated with MS development⁴⁵ interfere with the ability of NK cells to promote TRAIL-driven anti-inflammatory mechanisms in astrocytes.

In agreement with previous reports^{34,35}, we found that the commensal gut flora licenses IFN γ expression in NK cells, which migrate to the meninges and induce TRAIL-dependent

anti-inflammatory mechanisms in astrocytes. These findings suggest that in the basal state, activation of NK cells by the gut microbiota supports TRAIL⁺ anti-inflammatory astrocytes—identifying a novel role for microbiome-modulated IFN γ ⁺ NK cells in the regulation of CNS inflammation. Taken together with previous studies⁴⁶ that have shown that recirculating IgA B cells limit CNS inflammation through IL-10, our results highlight migratory immune cells as key components of the gut–CNS axis⁴⁷.

T cells are a major source of IFN γ in the CNS during EAE and MS⁴⁸, but T cells²⁹ and microglia¹⁵ also express molecules that limit the expression of TRAIL in astrocytes, as exemplified by the expression of GM-CSF in pathogenic IFN γ ⁺ T cells^{49,50}. Moreover, GM-CSF drives transcriptional modules in MAFG⁺ astrocytes that promote MS pathology¹⁶. Hence, although LAMP1⁺TRAIL⁺ astrocytes may not directly control GM-CSF-driven MAFG⁺ subsets of pathogenic astrocytes¹⁶, LAMP1⁺TRAIL⁺ astrocytes could indirectly limit the number and function of MAFG⁺ pathogenic astrocytes in EAE by inducing apoptosis in GM-CSF⁺ T cells. Considering the spatial heterogeneity of astrocyte subsets⁵¹, alterations in the balance between homeostatic and pathogenic astrocyte responses might be region-specific, highlighting the potential plasticity of transcriptional responses in astrocytes and their control by astrocyte–immune cell communication.

In summary, we have identified a subset of anti-inflammatory TRAIL⁺ astrocytes that limits CNS inflammation by inducing T cell apoptosis, and which is driven by meningeal IFN γ ⁺ NK cells that are licensed by the microbiome. Our findings define a previously unknown mechanism through which the microbiome regulates inflammation in the CNS, and identify targets for the therapeutic modulation of astrocytes in MS and other neurological diseases.

Online content

Any methods, additional references, Nature Research reporting summaries, source data, extended data, supplementary information, acknowledgements, peer review information; details of author contributions and competing interests; and statements of data and code availability are available at <https://doi.org/10.1038/s41586-020-03116-4>.

Methods

Data reporting

No statistical methods were used to predetermine sample size.

Mice

Mice were housed two to five animals per cage under a standard light cycle (12 h:12 h light:dark) (lights on from 07:00 to 19:00) at 20–23 °C and humidity (~50%) with ad libitum access to water and food. Adult female mice 8–10 weeks old and P0–P3 pups were used on a C57Bl/6J background (The Jackson Laboratory, 000664). Adult Tg(*Aldh111*-EGFP,-DTA) D8Rth/J (The Jackson Laboratory, 026033) were used for surface molecule screens. B6N.FVB-Tg(*Aldh111-creERT2*)1Khakh/J mice (The Jackson Laboratory, 029655) were bred to B6.Cg-Gt(ROSA)26Sortm 9(CAG-tdTomato)Hze/J mice (The Jackson Laboratory, 007909) to generate *Aldh111^{creERT2}tdTomato* mice. Cre expression was induced in

Aldh111^{creERT2tdTomato} mice by tamoxifen gavage at 6 weeks of age at a concentration of 200 mg kg⁻¹. Tamoxifen (Sigma-Aldrich, T5648) was diluted in corn oil (Sigma-Aldrich, C8267). One month after gavage, EAE was induced. B6.129S7-*Ifngr1^{tm1Agt}*/J mice (The Jackson Laboratory, 003288), B6.129S-*Tnfrsf1a^{tm1Imx}*, *Tnfrsf1b^{tm1Imx}*/J mice (The Jackson Laboratory, 003243), and *Aldh111-creERT2-Csf2rb^{ff}* mice were used for EAE experiments. B6.129S7-*Ifng^{tm1Ts}*/J mice (The Jackson Laboratory, 002287) mice were used for NK cell adoptive transfer experiments. Tg(CAG-Kaede)15Kgwa mice on a C57Bl/6J background were obtained from RIKEN BRC, Japan and used for antibiotic treatment and faecal microbiota transplant studies. C.129S4(B6)-*Ifng^{tm3.1Lky}*/J mice on a C57Bl/6J background were a gift from T. Korn (Technical University of Munich) and were used for analysis of NK cells in the meninges as well as antibiotic treatment and faecal microbiota transplant studies. Germ-free mice were bred in-house in tightly controlled and monitored isolators (Class Biologically Clean company) in an animal facility specifically dedicated to housing germ-free mice in the Massachusetts Host-Microbiome Center at the Brigham and Women's Hospital. All mice were housed in sterile autoclaved cages with irradiated food and acidified, autoclaved water. Mouse handling and weekly cage changes were performed by investigators or mouse husbandry staff wearing sterile gowns, masks and gloves in a sterile biosafety hood. Specific pathogen-free (SPF) mice used as controls were kept in the same mouse facility. All other SPF mice were kept in a facility at the Hale Building of Transformative Medicine at the Brigham and Women's Hospital in accordance with IACUC guidelines. All mice were 8–10 weeks old at the time of EAE induction, stereotactic injection, adoptive transfer of NK cells, or microbiota depletion and reconstitution. All procedures were reviewed and approved under the IACUC guidelines at Brigham and Women's Hospital.

Microbiota depletion and recolonization

To deplete the commensal flora, mice were administered an antibiotic cocktail for two weeks consisting of ampicillin (0.5 mg ml⁻¹, Sigma-Aldrich, A9518-25G), gentamicin (0.5 mg ml⁻¹, Sigma-Aldrich, PHR1077-1G), metronidazole (0.5 mg ml⁻¹, Sigma-Aldrich, M1547-5G), neomycin (0.5 mg ml⁻¹, Sigma-Aldrich, N1876-25G), and vancomycin (0.25 mg ml⁻¹, Sigma-Aldrich, V2002-5G) diluted in water containing saccharin (4 mg ml⁻¹, Sigma-Aldrich, 240931-1G). After two weeks, a randomly selected cohort of antibiotic-treated mice was orally gavaged with 200 µl of a freshly prepared faecal slurry containing 8 × 10⁸ CFU ml⁻¹ of bacteria, similar to a previously described approach⁵², and antibiotics were removed from the drinking water of recolonized mice. Antibiotic-treated mice were gavaged with faeces from the antibiotic-treated group. Recolonized mice were only gavaged with faeces from their same genotype. Reconstitution efficiency was assessed 4 days post-transplant by performing qPCR of bacterial 16S rRNA, similar to methods previously described⁵³. In brief, DNA was isolated from faeces through purification using a DNeasy PowerSoil Kit (Qiagen, 12888-100) and DNA was quantified using a Quant-iT dsDNA Assay Kit, high sensitivity (Thermo Fisher Scientific, Q33120). Normalized amounts of DNA were used as input for qPCR of 16S rRNA levels using Fast SYBR Green Master Mix (Thermo Fisher Scientific, 4385612). The 16S rRNA primers used were UniF340:5'-ACTCCTACGGGAGGCAGCAGT-3' and UniR514: 5'-ATTACCGCGGCTGCTGGC-3'. Downstream analyses were performed 10 days after reconstitution.

In vivo photoconversion of CAG^{Kaede} mice

For photoconversion of the small intestine, mice were briefly anaesthetized. The surrounding tissue was covered with sterile aluminium foil and a small opening was made in the peritoneal cavity, the small intestine was extended and exposed to 405-nm violet light using a 200 mW Electra Pro portable laser (Laserglow Technologies, GEL200XXX) for a total time of 2 min over the whole intestinal surface with continuous application of PBS on the exposed small intestine. After careful returning of the intestine to the peritoneal cavity, the peritoneum was closed with absorbable sutures and the skin was closed with surgical staples. Mice were euthanized 24, 48 or 72 h later for analysis of photoconverted red protein biodistribution by FACS.

EAE

EAE was induced as described^{16,25}. All mice used were on the C57Bl/6J background. EAE was induced using 150 µg of MOG₃₅₋₅₅ (Genemed Synthesis, 110582) mixed with freshly prepared complete Freund's Adjuvant (using 20 ml Incomplete Freund's Adjuvant (BD Biosciences, BD263910) mixed with 100 mg *Myobacterium tuberculosis* H-37Ra (BD Biosciences, 231141)) at a ratio of 1:1 (v/v at a concentration of 5 mg ml⁻¹). All mice received 2 subcutaneous injections of 100 µl each of the MOG/CFA mix. All mice then received a single intraperitoneal injection of pertussis toxin (List Biological Laboratories, 180) at a concentration of 2 ng µl⁻¹ in 200 µl of PBS. Mice received a second pertussis toxin injection at the same concentration two days after the initial EAE induction. Mice were monitored and scored daily thereafter. EAE clinical scores were defined as follows: 0, no signs; 1, fully limp tail; 2, hindlimb weakness; 3, hindlimb paralysis; 4, forelimb paralysis; 5, moribund; as described previously^{16,20,22,25,54}. Mice were randomly assigned to treatment groups. All mice were scored blind to genotype.

Lentivirus production

Lentiviral constructs were generated by modifying the pLenti-U6-sgScramble-Gfp-Cas9-2A-EGFP-WPRE lentiviral backbone as previously described^{16,25}. This backbone contains derivatives of the previously described reagents lentiCRISPR v2 (a gift from F. Zhang, Addgene plasmid 52961⁵⁵), and lentiCas9-EGFP (a gift from P. Sharp and F. Zhang, Addgene plasmid 63592⁵⁶). The *Gfp* promoter is the ABC₁D *gfa2* *GFAP* promoter⁵⁷. Substitution of sgRNAs was performed through a PCR-based cloning strategy using Phusion Flash HF 2X Master Mix (Thermo Fisher Scientific, F548L). A three-way cloning strategy was developed to substitute sgRNAs using the following primers: U6-PCR-F 5'-AAAGGCGCGCCGAGGGCCTATTT-3', U6-PCR-R 5'-TTTTTTGGTCTCCCGGTGTTTCGTCCTTCCAC-3', cr-RNA-F 5'-AAAAAAGGTCTCTACCG(N₂₀)GTTTTAGAGCTAGAAATAGCAAGTT-3', cr-RNA-R 5'-GTTCCCTGCAGGAAAAAAGCACCGA-3', in which N₂₀ marks the sgRNA substitution site. Amplicons were purified using the QIAquick PCR Purification Kit (Qiagen, 28104) and digested using DpnI (NEB, R0176S), BsaI-HF (NEB, R3535/R3733), AscI (for U6 fragment) (NEB, R0558), or SbfI-HF (for crRNA fragment) (NEB, R3642). pLenti backbone was cut with AscI and SbfI-HF and purified using the QIAquick PCR purification kit. Ligations were performed overnight at 16 °C using T4 DNA Ligase Kit

(NEB, M0202L). Ligations were transformed into NEB Stable Cells (NEB, C3040) at 37 °C, single colonies were picked, and DNA was prepared using QIAprep Spin Miniprep Kit (Qiagen, 27104). Lentiviral plasmids were transfected into HEK293FT cells according to the ViraPower Lentiviral Packaging Mix protocol (Thermo Fisher Scientific, K497500) and lentiviruses were packaged with pLP1, pLP2, and pseudotyped with pLP/VSVG. Medium was changed the next day, lentivirus was collected 48 h later and concentrated using Lenti-X Concentrator (Clontech, 631231) overnight at 4 °C followed by centrifugation according to the manufacturer's protocol and resuspension in 1/100-1/500 of the original volume in 1× PBS. Delivery of lentiviruses via intracerebroventricular (ICV) injection was performed largely as described previously^{4,16,20,22,25,37}. In brief, mice were anaesthetized using 1–3% isoflurane mixed with oxygen. Heads were shaved and cleaned using 70% ethanol and Betadine (Thermo Fisher Scientific, 19-027132) followed by a medial incision of the skin to expose the skull. The ventricles were targeted bilaterally using the coordinates: ±1.0 (lateral), –0.44 (posterior), –2.2 (ventral) relative to Bregma. Mice were injected with approximately 10⁷ total IU of lentivirus delivered by two 10 µl injections using a 25 µl Hamilton syringe (Sigma-Aldrich, 20787) on a Stereotaxic Alignment System (Kopf, 1900), sutured, and permitted to recover in a separate clean cage. Mice were permitted to recover for between 4 and 7 days before induction of EAE. CRISPR–Cas9 sgRNA sequences were designed using a combination of the Broad Institute's sgRNA GPP Web Portal (<https://portals.broad-institute.org/gpp/public/analysis-tools/sgrna-design>), Synthego (<https://design.synthego.com/#/validate>), and cross-referenced with activity-optimized sequences contained within the Addgene library 1000000096 (a gift from D. Sabatini and E. Lander)⁵⁸. sgRNAs used in this study were: sgLamp1: 5'-TGGCGCCTCAGCACTCTTTG-3', sgTnfsf10: 5'-ACTTCTCTCCACCCAGCTGC-3', sgIfngr1: 5'-GGTATTTCCAGCATAACGACA-3', sgIfngr2: 5'-GTGAAGCCTTGGGTTTCAGAG-3', sgStat1: 5'-GAGGAGGTCATGGAAGCGGA-3', and sgScramble: 5'-GCACTACCAGAGCTAACTCA-3' (sequence from Origene, GE100003).

Isolation of mouse CNS cells

CNS cells were isolated by flow cytometry as described^{4,16,20,22,25} and by modifying a previously described protocol⁵⁹. In brief, mice were perfused with 1× PBS, the CNS was isolated and finely minced, and incubated in 10 ml of enzyme digestion solution consisting of 75 µl Papain suspension (Worthington, LS003126) diluted in enzyme stock solution (ESS) and equilibrated to 37 °C. ESS consisted of 10 ml 10× EBSS (Sigma-Aldrich, E7510), 2.4 ml 30% D(+)-Glucose (Sigma-Aldrich, G8769), 5.2 ml 1M NaHCO₃ (VWR, AAJ62495-AP), 200 µl 500 mM EDTA (Thermo Fisher Scientific, 15575020), and 168.2 ml ddH₂O, filter-sterilized through a 0.22-µm filter. Samples were shaken at 80 rpm for 30–40 min at 37 °C. Enzymatic digestion was stopped with 1 ml of 10× hi ovomucoid inhibitor solution and 20 µl 0.4% DNase (Worthington, LS002007) diluted in 10 ml inhibitor stock solution (ISS). 10× hi ovomucoid inhibitor stock solution contained 300 mg BSA (Sigma-Aldrich, A8806), 300 mg ovomucoid trypsin inhibitor (Worthington, LS003086) diluted in 10 ml 1× PBS and filter sterilized using at 0.22-µm filter. ISS contained 50 ml 10× EBSS (Sigma-Aldrich, E7510), 6 ml 30% D(+)-Glucose (Sigma-Aldrich, G8769), 13 ml 1M NaHCO₃ (VWR, AAJ62495-AP) diluted in 170.4 ml ddH₂O and filter-sterilized through a 0.22-µm filter. Tissue was mechanically dissociated using a 5 ml serological pipette and

filtered through at 70- μ m cell strainer (Thermo Fisher Scientific, 22363548) into a fresh 50-ml conical. Tissue was centrifuged at 500g for 5 min and resuspended in 10 ml of 30% Percoll solution (9 ml Percoll (GE Healthcare Biosciences, 17-5445-01), 3 ml 10 \times PBS, 18 ml ddH₂O). For analysis of spinal cords in *Aldh111^{creERT2tdTomato}* mice, Percoll was not used owing to heavy myelination of the tissue. The Percoll suspension was centrifuged at 500g for 25 min with no brakes. Supernatant was discarded and the cell pellet was washed 1 \times PBS, centrifuged at 500g for 5 min and prepared for downstream applications.

Isolation of mouse splenic cells

Spleens were isolated before mouse perfusion and mechanically dissociated. Red blood cells were lysed with ACK lysing buffer (Life Technology, A10492-01) for 5 min and washed with 0.5% BSA, 2 mM EDTA pH 8.0 in 1 \times PBS and prepared for downstream applications.

Astrocyte FACS analysis

Cells were stained for 30–60 min in the dark on ice, then cells were washed with PBS and resuspended in 0.5% BSA and 2 mM EDTA pH 8.0, in 1 \times PBS for sorting or flow cytometry analysis as previously described^{4,16,20,22,25}. For astrocyte surface marker screening, CNS cells derived from Tg(Aldh111-EGFP,-DTA)D8Rth/J mice were plated on LegendScreen Mouse PE kit plates (BioLegend, 700005) containing 266 pre-titrated antibodies including 255 PE-conjugated antibodies and 11 isotype controls, arrayed on three 96-well plates, with one antibody per well. Cells were resuspended at a concentration of 4 \times 10⁶ and 1 \times 10⁷ cells per ml in accordance with the manufacturer's protocol and plated equally between the three 96-well plates. Cells were incubated with 405 Aqua LIVE/DEAD cell stain kit (L34966, Thermo Fisher Scientific, 1:400) and stained with each PE-conjugated antibody according to the manufacturer's protocol. Cells were then washed times with 1 \times PBS and stained intracellularly for EGFP using the intracellular antibody labelling kit (eBioscience, 00-5523) and a rabbit anti-GFP antibody, ChIP grade (Abcam, ab290, 1:150) for 15 min on ice. Cells were washed 3 times and incubated with goat anti-rabbit IgG (H+L) highly cross-adsorbed secondary antibody, Alexa Fluor 488 (Thermo Fisher Scientific, A-11034, 1:500) for 15 min on ice. Cells were then washed 3 times and analysed using a BD HTS on an LSRII (BD Biosciences).

For flow cytometry analyses the following antibodies were used: BUV737 anti-mouse CD11b (BD Biosciences, 564443, 1:100), PE/Dazzle594 anti-mouse CD29 (Biolegend, 102231, 1:100), PerCP-eFluor 710 anti-mouse CD39 (eBioscience, 46-0391-82, 1:100), BUV661 anti-mouse CD45 (BD Biosciences, 565079, 1:100), BV650 anti-mouse CD49a (BD Biosciences, 740519, 1:100), BV421 anti-mouse CD66a (Biolegend, 134531, 1:100), APC anti-mouse CD84 (Miltenyi, 130-102-592, 1:10), BV786 anti-mouse CD88 (BD Biosciences, 743774, 1:100), PE-Cy7 anti-mouse CD98 (Biolegend, 128214, 1:100), BV605 anti-mouse CX3CR1 (BioLegend, 149027, 1:100), BUV395 anti-mouse LAMP1 (BD Biosciences, 565533, 1:100), APC-R700 anti-mouse CD184 (BD Biosciences, 565522, 1:100), fluorescein isothiocyanate (FITC) anti-mouse ESAM (Biolegend, 136205, 1:100), APC-Cy7 anti-mouse Ly6AE (BD Biosciences, 560654, 1:100), BV570 anti-mouse Ly6C (Biolegend, 128030, 1:100), BUV563 anti-mouse Ly6G (BD Biosciences, 565707, 1:100) and live/dead cell marker (Thermo Fisher Scientific, L34966). Compensation was performed

on single-stained beads (Thermo Fisher Scientific, 01-2222-42). Astrocytes isolated from *Aldh111^{creERT2}TdTomato* mice were gated as tdTomato⁺CX3CR1⁻ cells and 50,000 live astrocytes were acquired on a Symphony A5 (BD Biosciences).

T cell FACS analysis

To analyse T cell populations, CNS and splenic cell suspensions were stimulated with 50 ng ml⁻¹ phorbol 12-myristate 13-acetate (PMA, Sigma-Aldrich, P8139), 1 μM ionomycin (Sigma-Aldrich, I3909-1ML), GolgiStop (BD Biosciences, 554724, 1:1500) and GolgiPlug (BD Biosciences, 555029, 1:1,500) diluted in T cell culture medium (RPMI (Life Technologies, 11875119) containing 10% FBS, 1% penicillin/streptomycin, 50 μM 2-metcaptoethanol (Sigma-Aldrich, M6250), and 1% non-essential amino acids (Life Technologies, 11140050)). After 4 h, cell suspensions were washed with 0.5% BSA, 2 mM EDTA in 1× PBS and incubated with surface antibodies and a live/dead cell marker on ice. After 30 min, cells were washed with 0.5% BSA, 2 mM EDTA in 1× PBS and fixed according to the manufacturer's protocol of an intracellular labelling kit (eBiosciences, 00-5523-00). Surface antibodies used in this study were: BUV661 anti-mouse CD45 (BD Biosciences, 565079, 1:100), BV750 anti-mouse CD3 (Biolegend, 100249, 1:50), PE-Cy7 anti-mouse CD4 (eBioscience, 25-0041-82, 1:100), BUV737 anti-mouse CD11b (BD Biosciences, 564443, 1:100), BV570 anti-mouse Ly6C (Biolegend, 128030, 1:100), BUV805 anti-mouse CD8a (BD Bioscience, 564920, 1:100), BUV563 anti-mouse Ly6G (BD Biosciences, 565707, 1:100), BUV737 anti-mouse CD11c (BD Biosciences, 612797, 1:100), Pe-Cy5 anti-mouse CD44 (BioLegend, 103010, 1:100), PerCP-Vio700 anti-mouse DR5 (Miltenyi, MD5-1-3C2, 1:10), BV421 anti-mouse NK1.1 (BD Biosciences, 562921, 1:100). Intracellular antibodies were: APC-Cy7 anti-mouse IFNγ (BD Biosciences, 561479, 1:100), PE anti-mouse IL-17A (eBiosciences, 12-7177-81, 1:100), BV421 anti-mouse GM-CSF (BD Biosciences, 564747, 1:100), FITC anti-mouse FOXP3 (eBiosciences, 11-5773-82, 1:100), BV605 anti-active-caspase 3 (BD Biosciences, 564094, 1:20). For all in vivo studies, active-caspase 3 was analysed using CellEvent Caspase-3/7 Green Flow Cytometry Assay Kit (Invitrogen, C10427). Gating of CNS and splenic cells was performed on more than 50,000 live CD3⁺CD4⁺ cells. FACS was performed on a Symphony A5 (BD Biosciences).

Flow cytometry

For analysis of astrocytes derived from *Aldh111^{creERT2}TdTomato* reporter mice, CNS cells were stained with APC anti-mouse LAMP1 (BioLegend, 121614, 1:100) and PE-Cy7 anti-mouse TRAIL (BioLegend, 109311, 1:100) for 45 min on ice. Cells were washed with 0.5% BSA, 2mM EDTA in 1× PBS and resuspended in 1× PBS for sorting. For analysis of astrocytes derived from C57Bl/6J mice, antibodies used were: PE anti-mouse CD45R/B220 (BD Biosciences, 553089, 1:100), PE anti-mouse TER-119 (BioLegend, 116207, 1:100), PE anti-O4 (R&D Systems, FAB1326P, 1:100), PE anti-CD105 (eBiosciences, 12-1051-82, 1:100), PE anti-CD140a (eBiosciences, 12-1401-81, 1:100), PE anti-Ly6G (BioLegend, 127608, 1:100), BV786 anti-Ly6C (BioLegend, 128041, 1:100), APC anti-CD45 (eBiosciences, 17-0451-83, 1:100), APC-Cy7 anti-CD11c (BD Biosciences, 561241, 1:100), BV650 anti-CD3 (BD Biosciences, 740530, 1:100), and FITC anti-CD11b (eBiosciences, 11-0112-85, 1:100). All cells were gated with the following parameters: CD105/CD140/O4/

Ter119/Ly6G/B220⁻. For caspase-3/7 evaluation, cells were washed with 0.5% BSA, 2 mM EDTA in 1× PBS and incubated with surface antibodies and a live/dead cell marker on ice for 30 min. After, cells were washed and following staining for Caspase-3/7 according to the manufacturer's instructions (Invitrogen, C10427). FACS analysis was performed on a Symphony A5 (BD Biosciences). Surface antibodies used were: BUV395 anti-mouse CD69 (BD Biosciences, 740220, 1:100), BUV661 anti-mouse CD45 (BD Biosciences, 565079, 1:100), BUV805 anti-mouse CD8a (BD Bioscience, 564920, 1:100), BV750 anti-mouse CD3 (Biolegend, 100249, 1:50), PE-Cy7 anti-mouse CD4 (eBioscience, 25-0041-82, 1:100), BV786 anti-mouse CD11b (BD Biosciences, M1/70, 1:100), and PerCP-Vio700 anti-mouse DR5 (Miltenyi, MD5-1-3C2, 1:10). For knockdown validation, CNS cells were washed with 0.5% BSA, 2 mM EDTA in 1X PBS and incubated with surface antibodies and a live/dead cell marker on ice. After 1 h, cells were washed and incubated with secondary antibody AF647 AffiniPure Fab Fragment Donkey anti-rabbit IgG (Jackson ImmunoResearch, 711-607-003, 1:500) for 30 min on ice. Then, cells were washed 3 times with 0.5% BSA, 2mM EDTA in 1× PBS, fixed according to the manufacturer's protocol of an intracellular labelling kit (eBiosciences, 00-5523-00) and incubated with intracellular antibodies: BV421 anti-mouse GFAP (BioLegend, 644710, 1:100), PE-CF594 anti-mouse STAT1 (BD Biosciences, 562674, 1:20), and rabbit anti-GFP antibody, CHIP Grade (Abcam, ab290, 1:150) for 45 min at room temperature, washed and incubated with a goat anti-rabbit IgG (H +L) Alexa Fluor 488 highly cross-adsorbed secondary antibody (Thermo Fisher Scientific, A-11034, 1:500) for 30 min on room temperature. Cells were washed 3 times with 0.5% BSA, 2 mM EDTA in 1× PBS and resuspended in 1× PBS FACS analysis performed on a Symphony A5 (BD Biosciences). Surface antibodies used were: BUV395 anti-mouse LAMP1 (BD Biosciences, 1D4B, 1:100), BUV661 anti-mouse CD45 (BD Biosciences, 565079, 1:100), BV605 anti-mouse CX3CR1 (BioLegend, 149027, 1:100), BV650 anti-mouse IFNGR1/CD119 (BD Biosciences, 740498, 1:100), BV786 anti-mouse CD11b (BD Biosciences, M1/70, 1:100), PE-Cy7 anti-mouse CD253 (TRAIL) (BioLegend, N2B2, 1:100) and anti-mouse IFNGR2 (Invitrogen, PA5-109847, 1:50). Astrocytes were sorted as CD45/CD11b/Ly6C/CD11c⁻. Microglia were sorted as CD45^{low}CD11b^{high}Ly6C^{low}. Pro-inflammatory monocytes were sorted as CD45^{high}CD11b^{high}Ly6C^{high}. Compensation was performed on single-stained beads. Cells were sorted on a FACS Aria Ilu (BD Biosciences).

Primary astrocyte and microglia cultures

Procedures were performed largely as described previously^{4,16,22,25}. Brains of mice aged P0–P3 were dissected into PBS on ice. Brains were centrifuged at 500g for 10 min at 4 °C and resuspended in 0.25% Trypsin-EDTA (Thermo Fisher Scientific, 25200-072) at 37 °C for 10 min. DNase I (Thermo Fisher Scientific, 90083) was then added at a concentration of 1 mg ml⁻¹ to the solution, and the brains were digested for 10 more minutes at 37 °C. Trypsin was neutralized by adding DMEM/F12+GlutaMAX (Thermo Fisher Scientific, 10565018) supplemented with 10% FBS (Thermo Fisher Scientific, 10438026) and 1% penicillin–streptomycin (Thermo Fisher Scientific, 15140148), and cells were passed through a 70-µm cell strainer. Cells were centrifuged at 500g for 10 min at 4 °C, resuspended in DMEM/F12+GlutaMAX with 10% FBS/1% penicillin–streptomycin and cultured in T-75 flasks (Falcon, 353136) pre-coated with poly-L-lysine (Sigma Aldrich, P4707) for 1 h at 37 °C and washed with 1× PBS. Cells were cultured at 37 °C in a

humidified incubator with 5% CO₂, for 7–10 days until confluency was reached. Medium was replaced every 2–3 days. Microglia were removed by shaking for 30 min at 180 rpm, and the medium was changed, then cells astrocytes were shaken for 2 h at 220 rpm and the medium was changed again. Remaining attached cells were enriched astrocytes. To obtain microglia, medium was centrifuged at 500g for 5 min at 4 °C, pellet was resuspended in 0.5% BSA, 2mM EDTA in 1× PBS, and magnetic sorted using anti-mouse CD11b microbeads according to the manufacturer's protocol (Miltenyi, 130-049-601).

Primary neuron cultures

Primary pyramidal neurons from the cortex and hippocampus were cultured as previously described⁶⁰. In brief, the brains of P0 mice were isolated, the cortices and hippocampi were isolated and plated into freshly prepared sterile dissection medium. Dissection medium contained sodium pyruvate (diluted to 1×, Invitrogen, 11360070), 0.1% glucose (Sigma-Aldrich, G-6152), 10 mM HEPES (Invitrogen, H-4034), diluted in Ca²⁺/Mg²⁺-free HBSS (Invitrogen, 14175095). Tissue was then resuspended in 0.25% trypsin solution in dissection medium and incubated at 37 °C for 20 min. DNase solution was added for 5 min at room temperature. Tissue was washed twice with dissection medium, then washed twice with plating medium. Plating medium contained 10% FBS, 0.45% glucose, 1mM sodium pyruvate, 2 mM glutamine (Invitrogen, 25030081), and penicillin–streptomycin (diluted to 1×, Invitrogen, 15140122) in MEM Eagle's with Earle's BSS (Invitrogen, 21010046). Tissue was dissociated using a pipette, then plated on poly-L-lysine-coated glass coverslips (Sigma-Aldrich, P2636). Neurons were maintained in maintenance medium containing B-27 (Invitrogen, 17504044), 2 mM glutamine, and penicillin–streptomycin diluted in neurobasal medium (Invitrogen, 21103049). Neurons were cultured for 10 days with medium changed every 2 days, then used for pharmacological analyses.

Primary astrocyte cytokine stimulation

Cytokine treatment was performed for 10 h with cytokines diluted in DMEM/F12+GlutaMAX (Life Technologies, 10565042) supplemented with 10% FBS (Life Technologies, 10438026) and 1% penicillin–streptomycin (Life Technologies, 15140122). The following recombinant cytokines were used to stimulate astrocytes: 100 ng ml⁻¹ IFN γ (R&D Systems, 485-MI-100), 5 ng ml⁻¹ TNF (R&D Systems, 410-MT-010), 10 ng ml⁻¹ IL-1 β (R&D Systems, 401-ML-005), 500 UI ml⁻¹ IFN β (R&D Systems, 8234-MB-010/CF), 10 ng ml⁻¹ IL-10 (R&D Systems, 417-ML-005), 10 ng ml⁻¹ TGF β (Miltenyi, 130-095-067), 10 ng ml⁻¹ IL-17 (R&D Systems, 421-ML-025/CF), 200 ng ml⁻¹ GM-CSF (PeproTech, 315-03), 25 ng ml⁻¹ IL-27 (Sigma-Aldrich, SRP4187-10UG). For siRNA transfections, 1.5 μ l of a 20 μ M siRNA pool was mixed with 2 μ l interferin (Polyplus-transfection, 409-10) in 100 μ l Opti-MEM (Life Technologies, 31985062). The mix was incubated for 10 min at room temperature and added to a well of a 24-well plate containing 500 μ l of astrocyte medium. Forty-eight hours later, cells were used for downstream assays. siRNA pools used were siTnfsf10 (Dharmacon, L-047370-00-0005), siLamp1 (Dharmacon, L-048173-00-0005) and siScrambl (Dharmacon, D-001810-10-20).

RNA isolation from cultured mouse astrocytes

Primary astrocytes were lysed in Buffer RLT (Qiagen) and RNA was isolated from cultured astrocytes using the Qiagen RNeasy Mini kit (Qiagen, 74106). cDNA was transcribed using the High-Capacity cDNA Reverse Transcription Kit (Life Technologies, 4368813). Gene expression was then measured by qPCR using Taqman Fast Universal PCR Master Mix (Life Technologies, 4367846). Taqman probes used in this study are: *Gapdh* (Mm99999915_g1), *Tnfrsf10* (Mm01283606_m1), *Ifng* (Mm01168134_m1), *Fasl* (Mm00438864_m1), *Gzmb* (Mm00442834_m1), *Prfl* (Mm00812512_m1), *Cxcr3* (Mm99999054_s1), *Ccr6* (Mm99999114_s1), *Ccr1* (Mm00438260_s1), *Ccr5* (Mm01963251_s1), *Ccr4* (Mm01963217_u1), *Ccl5* (Mm01302427_m1), *Cxcl12* (Mm00445553_m1), *Ccl20* (Mm01268754_m1), *Ccl3* (Mm00441259_g1), *Ccl22* (Mm00436439_m1), *Psmb8* (Mm00440207_m1), *Psmb9* (Mm00479004_m1), and *Lamp1* (Mm00495262_m1). qPCR data were analysed by the ddCt method by normalizing the expression of each gene for each replicate to *Gapdh* and then to the control group.

Enzyme-linked immunosorbent assay

CNS and/or spleen cells were cultured with MOG₃₅₋₅₅ for 48 h, and supernatant was collected. Costar 96-well plates (Corning, 3690) were coated with capture antibodies diluted in 1× PBS: anti-mouse GM-CSF Capture (Invitrogen, 88-7334-88, 1:250), anti-mouse IL-10 capture (Invitrogen, 88-7105-88, 1:250), purified anti-mouse IFN γ (BD Biosciences, 551309, 1:500), and purified anti-mouse IL-17A (BD Biosciences, 555068, 1:500) overnight at 4 °C. Plates were washed twice with 0.05% Tween in 1× PBS (Boston BioProducts, IBB-171X) and blocked with 1% BSA in 1× PBS (Thermo Fisher Scientific, 37525) for 2 h at room temperature. Standard curve was prepared from 2 $\mu\text{g ml}^{-1}$ diluted in 1× Elispot diluent (eBioscience, 00-4202-56). Samples were diluted in 1× Elispot diluent 4× to IFN γ , 2× to GM-CSF and IL-17A, and not diluted for IL-10. Plates were washed twice with 0.05% Tween in 1× PBS and samples and standard curve were added and incubated overnight at 4 °C. The next day, plates were washed 5 times with 0.05% Tween in 1× PBS and incubated with detection antibodies diluted in 1× Elispot diluent: anti-mouse GM-CSF Detection (Invitrogen, 88-7334-88, 1:250), anti-mouse IL-10 detection (Invitrogen, 88-7105-88, 1:250), biotin anti-mouse IFN γ (BD Biosciences, 554410, 1:500), and biotin anti-mouse IL-17A (BD Biosciences, 555067, 1:500) shaken for 1 h at room temperature. Afterwards, plates were washed 8 times with 0.05% Tween in 1× PBS and incubated with Avidin-HRP diluted in 1× Elispot diluent (Invitrogen, 88-7334-88, 1:250) shaken for 1 h at room temperature. Next, plates were washed 8× with 0.05% Tween in 1× PBS and revealed using 1× TMB Substrate Solution (Invitrogen, 00-4201-56). The reaction was stopped by KPL TBM Stop Solution (SeraCare, 5150-0021) and plates were read at 450 nm on Glo-Max Explorer Multimode Microplate Reader (Promega).

Recall response

For recall responses, splenocytes were cultured in complete RPMI medium for 72 h at a density of 4×10^5 cells per well in 96-well plates in the presence of MOG₃₅₋₅₅ peptide (Genemed Synthesis, 110582). During the final 16 h, cells were pulsed with 1 μCi [3H]-thymidine (PerkinElmer, NET027A005MC) followed by collection on glass fibre filters

(PerkinElmer, 1450-421) and analysis of incorporated [3H]-thymidine in a β -counter (PerkinElmer, 1450 MicroBeta TriLux).

FACS from cultured mouse astrocytes

For FACS, astrocytes were incubated with 0.25% trypsin-EDTA (Thermo Fisher Scientific, 25200-072) at 37 °C for 10 min, washed and stained with BUV395 anti-mouse LAMP1 and PE-Cy7 anti-mouse TRAIL antibody for 30 min on ice. For intracellular staining, cells were fixed according to the manufacturer's instructions (eBiosciences, 00-5523-00) and stained with PE anti-pSTAT1 (Ser727) (Biolegend, 686404). Cells were washed and analysed on an LSR Fortessa (BD Biosciences).

In silico promoter analysis

The *Mus musculus Tnfrsf10* genomic sequence was obtained using Ensembl⁶¹. The DNA sequences ~3,000 bp upstream of the protein coding transcripts *Tnfrsf10* were analysed. STAT1 DNA-binding sites were defined using Mulan⁶².

ChIP

Approximately 1 million astrocytes were treated overnight followed by cell preparation according to the ChIP-IT Express Enzymatic Shearing and ChIP protocol (Active Motif, 53009). In brief, cells were fixed in 1% formaldehyde for 10 min with gentle agitation, washed in 1× PBS, washed for 5 min in 1× glycine stop-fix solution in PBS, and scraped in 1X PBS supplemented with 500 μ M PMSF. Cells were pelleted, nuclei isolated, and chromatin sheared using the Enzymatic Shearing Cocktail (Active Motif) for 10 min at 37 °C with vortexing every 2 min. Sheared chromatin was immunoprecipitated according to the Active Motif protocol overnight at 4 °C with rotation. The next day, the protein-bound magnetic beads were washed once with ChIP buffer 1, once with ChIP buffer 2, and once with 1× TE. Cross-links were reversed in 100 μ l of 0.1% SDS and 300 mM NaCl in 1× TE at 63 °C for 4–5 h, as described^{16,25}. DNA was purified using QIAquick PCR Purification Kit (Qiagen, 28104). qPCR was performed using Fast SYBR Green Master Mix (Thermo Fisher Scientific, 4385612). Anti-IgG immunoprecipitation and input were used as controls. Antibodies used were mouse anti-pSTAT1 (Ser727) (BioLegend, 686414) and IgG1 isotype control (Abcam, ab171870). PCR primers were designed with Primer3⁶³ to generate 50–150 bp amplicons. Primer sequences used: STAT1-TRAIL1-F: 5' - CTAGGCTTTCCAGCACCATC-3', STAT1-TRAIL1-R: 5' - CAGTGCCTGAGAAGGTCACA-3', STAT1-TRAIL2-F: 5' -5' - ACAGCGTGGAGAAGAAAGGA-3', STAT1-TRAIL2-F: 5' - GGGTGCATGATGTGAAACAC-3'. Data were analysed by ddCt relative to IgG control.

Astrocyte-immune cell co-cultures

Naive CD4⁺ T cells and NK cells were isolated from the spleens of B6.SJL-Ptprca Pepcb/BoyJ mice (The Jackson Laboratory, 002014) or *Ifng^{EYFP}* reporter mice using Miltenyi beads (130-104-453 and 130-115-818). CD4⁺ T cells were activated overnight with 10 μ g ml⁻¹ anti-CD3 (bioXcell, BE0001-1-A005mg) and 0.25 μ g ml⁻¹ anti-CD28 (bioXcell, BE0015-5-A005mg). For co-culture with EAE T cells, T cells were isolated from mice

undergoing EAE at the peak of disease by flow cytometry based on CD3, CD4, and DR5 expression. DR5⁺ and DR5⁻ T cells were isolated separately for co-culture. Astrocytes and CD4⁺ T cells were co-cultured in a 2:1 ratio. To block TRAIL, astrocytes were treated with IFN γ overnight, washed extensively with 1 \times PBS, and 2.5 $\mu\text{g ml}^{-1}$ of anti-TRAIL antibody (Thermo Fisher Scientific, 16-5951-85) or isotype control antibody (Thermo Fisher Scientific, 16-4321-81). Astrocytes were incubated with antibodies for one hour before addition of activated CD4⁺ T cells. In another set of experiments CD4⁺ T cells were activated with anti-CD3 and anti-CD28 as described above for 72 h and NK cells were activated with 100 ng ml⁻¹ LPS (Invivogen, tlr1-3pelps) for 48 h. *Ifng*^{YFP+} and *Ifng*^{YFP-} cells were sorted and co-cultured with astrocytes. After 8 h of co-culture, cells were collected for FACS. Cell-surface antibodies were added for 30 min on ice, cells were washed and fixed to detect active-caspase-3 as described above. For TUNEL (Abcam, ab66108) staining, cells were fixed in 1% v/v PFA for 15 min on ice, washed with 1 \times PBS and incubated with 70% ethanol for 30 min on ice and washed twice. Cells were stained with staining solution (10 μl of reaction buffer, 0.75 μl of TdT enzyme, 8 μl of FITC-dUTP and 32.25 μl of water) for 60 min at 37 $^{\circ}\text{C}$, washed and acquired on LSR Fortessa (BD Biosciences) or Symphony A5 (BD Biosciences). Antibodies used were: BV711 anti-mouse CD45.1 (BD Biosciences, 747742, 1:100), PE/Dazzle594 anti-CD11b (Biolegend, 101256, 1:100), PE anti-mouse CD3 (Biolegend, 100206, 1:100), BV650 anti-mouse CD4 (Biolegend, 100546, 1:100), PerCP-Vio700 anti-mouse DR5 (Miltenyi, MD5-1-3C2, 1:10), APC-Cy7 anti-IFN γ (BD Biosciences, 561479, 1:100), PE anti-mouse IL-17A (eBioscience, 12-7177-81, 1:100), BUV395 anti-mouse LAMP1, PE-Cy7 anti-mouse TRAIL, BUV661 anti-mouse CD45, BV786 anti-mouse CD11b, BV421 anti-mouse NK1.1 and BV750 anti-CD3.

Immunostaining of CNS tissue

For WGA staining, mice were first intracardially injected with fluorescently labelled WGA (Biotium, 29026), for 3 min. Mice were intracardially perfused with ice cold 1 \times PBS followed by ice-cold 4% PFA. Spinal columns were collected, post-fixed in 4% PFA overnight at 4 $^{\circ}\text{C}$. For analysis of spinal column meningeal samples, spinal columns were transferred to 20% EDTA pH 7.4 (Thermo Fisher Scientific, S28291GAL) at 4 $^{\circ}\text{C}$ with inversion until bone was decalcified. Samples were then dehydrated in 30% sucrose for 2 days at 4 $^{\circ}\text{C}$. Spinal cords from naive or EAE mice were frozen in OCT (Sakura, 4583) and stored at -80°C . Twenty-micrometre sections were collected on SuperFrost Plus slides (Thermo Fisher Scientific, 22-037-246) using a cryostat and then baked at 60 $^{\circ}\text{C}$ for 15 min. A hydrophobic barrier was drawn on the slides around the tissue sections (Vector Laboratories, H-4000) and samples were washed 3 times for 10 min with 0.1% Triton X-100 in PBS (PBS-T). Sections were then permeabilized for 20 min using 0.3% Triton X-100 in PBS and washed 3 times for 10 min with PBS-T. After this, the endogenous peroxidase activity was quenched using 3% hydrogen peroxide solution for 30 min. Sections were washed 3 times for 10 min with PBS-T and then stained using goat anti-TRAIL (Thermo Fisher Scientific, PA5-47073, 1:100) or rat CD3e (Abcam, ab33429, 1:200). After staining, tissues were washed 3 times for 10 min with PBS-T. TRAIL and CD3e were detected using Alexa Fluor 568 donkey anti-goat IgG (Thermo Fisher Scientific, A-11057, 1:300) or Alexa Fluor 568 donkey anti-rat IgG (Abcam, ab175475, 1:300) respectively. After rinsing 3 times

for 10 min with PBS-T, sections were then stained using anti-IFN γ (Abcam, ab9657, 1:50), followed by detection using Tyramide Superboost Signal Amplification kit (Thermo Fisher Scientific, B40943) according to manufacturer's instructions, analogous to previous studies staining cytokines in tissues^{16,20,22,37,64-69}. Then sections were washed 3 times for 10 min with PBS-T and stained using mouse anti-GFAP (Millipore, MAB360, 1:200) or mouse anti-NK1.1 (BioLegend, 108701, 1:200). After staining, tissues were washed 3 times for 10 min with PBS-T followed by detection using Alexa Fluor 647 donkey anti-mouse IgG (Abcam, ab150107, 1:300). All primary antibodies were incubated overnight at 4 °C and all secondary antibodies were incubated for 2 h at room temperature. After all staining, tissues were washed 3 times for 10 min with PBS-T and 200 μ l of mounting medium with DAPI (SouthernBiotech, 0100-20) were added to the slides. Finally, tissues were covered with coverslips (VWR, 48404-111) and stored in the dark at 4 °C until imaging. For analysis of the distribution of lentiviral vectors throughout the CNS, 30 μ m sagittal sections of brain or axial sections of spinal cord were acquired. Primary antibodies used for these analyses were mouse anti-GFAP (Millipore, MAB360, 1:200) and chicken anti-GFP (Abcam, 13970, 1:500). Secondary antibodies used were goat anti-chicken IgY (H+L), Alexa Fluor 488 (Life Technologies A11039) and Alexa Fluor 647 donkey anti-mouse (Abcam, ab150107). Sections were imaged on an LSM710 Zeiss confocal or Leica DMI8 as described previously^{4,16,25}. Large image scans were acquired using the tiling function on the LSM710 or Leica DMI8. The number of TRAIL-expressing cells was quantified manually using the Cell Counter plug-in in FIJI. At least 100 cells per sample were counted. Expression was normalized to GFAP⁺ astrocyte cell number. TRAIL fluorescent intensity was also quantified within the meninges and parenchyma of individual spinal cord sections using FIJI.

Immunostaining of meninges

Mice were deeply anaesthetized using isoflurane and tested for absence of pinch reflex before the procedure. An incision was performed to expose the thoracic cavity, and 100 μ l of CF640R-conjugated wheat germ agglutinin (Biotium, 29026-1, stock concentration 1 mg ml⁻¹ in PBS) was injected into the left ventricle of the heart to stain blood vessels. After 5 min, mice were perfused with 20 ml of PBS followed by 20 ml of 4% PFA in 1 \times PBS. Samples of cortical meninges attached to the skull were collected, post-fixed for 24 h at 4 °C in 4% PFA, and decalcified in 20% EDTA solution for 48 h at room temperature. For staining, samples were treated with blocking solution (10% donkey serum, 0.1% Triton X-100 in PBS) for 24h at 4 °C, and stained with mouse anti-NK1.1 (BioLegend, 108702, 1:100) diluted in blocking solution for 24 h at 4 °C. Samples were washed with PBS for 24 h and stained with goat anti-mouse IgG H&L (Alexa Fluor 594) secondary antibody (Abcam, ab150116, 1:100) and 16 μ M Hoechst 33342 (Thermo Fisher Scientific, H3570) diluted in blocking solution for 24h. Stained samples were washed with 1 \times PBS for 24 h at 4 °C, and slides were prepared using Vectashield Mounting Medium (Vector Laboratories, H-1000). Fluorescence imaging was performed using a Nikon Ti2 confocal inverted microscope and images were acquired using NIS-Elements AR software.

Dissection of meningeal cells for flow cytometry

Mice were euthanized and received an intracardiac injection (into the left ventricle) of anti-mouse CD45-BV661 (3 μg in 50 μl of PBS). After 5 min, blood was removed by cutting the right atrium and the head was severed. The skin was removed from the head and a cut was made around the cranium (from the foramen magnum to the frontal bone) to dissect the bones of the calvarium. The calvarium was then transferred to a dissection scope and the meninges were removed. Tissue was incubated for 30 min at 37 °C in 500 μl of digestion mix composed of 0.5 mg ml^{-1} of collagenase P (Sigma-Aldrich, 11213865001), 0.5 mg ml^{-1} of dispase (Worthington, LS02104), and 125 U ml^{-1} of DNase I (Sigma-Aldrich, 10104159001) in RPMI-1640. After incubation, samples were washed, resuspended in 1 ml ice-cold 0.5% BSA, 2 mM EDTA in 1 \times PBS, and gently dissociated using a wide-bore 1 ml pipette tip. Finally, the cell suspension was filtered through a 40 μm FlowMi filter (Sigma-Aldrich, BAH136800040-50EA). Cell suspensions were stimulated with 50 ng ml^{-1} PMA, 1 μM ionomycin, GolgiStop and GolgiPlug diluted in T cell culture medium. After 4 h, cell suspensions were washed with 0.5% BSA, 2mM EDTA in 1 \times PBS and incubated with surface antibodies and live/dead cell marker on ice. After 30 min, cells were washed with 0.5% BSA, 2mM EDTA in 1 \times PBS and fixed according to the manufacturer's instructions for the intracellular antigen labelling kit (eBiosciences, 00-5523-00). Surface antibodies used were: BUV661 or PE-Cy5 (BD Biosciences, 553082) anti-mouse CD45, BV750 anti-mouse CD3, PE-Cy7 anti-mouse CD4, BUV737 anti-mouse CD11b, BV421 anti-mouse NK1.1, Alexa 647 anti-mouse CD200R (BD Biosciences, 566345, 1:100), BUV395 anti-mouse CD27 (BD Biosciences, 740247, 1:100), BUV737 anti-mouse CD11c, BUV805 anti-mouse CD8a, BV570 anti-mouse Ly-6C, BV650 anti-mouse CD62L (BD Biosciences, 564108, 1:100), BV711 anti-mouse CD127 (BD Biosciences, 565490, 1:100), BV786 anti-mouse CD11b, and APC-eFluor 780 anti-mouse CD335/NKp46 (Thermo Fisher Scientific, 47-3351-82, 1:100). Intracellular antibody used was APC-Cy7 anti-mouse IFN γ .

Human meninges staining

Use of tissues from patients with MS was approved by the Neuroimmunology Research Laboratory, Centre de Recherche du Centre Hospitalier de l'Université de Montréal (CRCHUM) under ethical approval number BH07.001. Human tissue was obtained from patients diagnosed with clinical and neuropathological MS according to the revised 2010 McDonald's criteria⁷⁰. Tissue samples were collected from healthy donors and patients with MS with full ethical approval (BH07.001) and informed consent as approved by the local ethics committee. Inflammatory infiltrates were defined as 5–50 loosely packed cells around blood vessels in the meninges. Frozen brain tissue from 3 patients with MS and 3 healthy control individuals was cut into 7- μm thick sections, air-dried, and fixed in ice-cold acetone for 10 min. Sections were de-lipidized in 70% ethanol for 5 min, followed by blocking of non-specific binding with 10% donkey serum (D9663, Sigma-Aldrich). Sections were then permeabilized for 20 min using 0.3% Triton X-100 in PBS and washed 3 times for 10 min with PBS-T. After this, the endogenous peroxidase activity was quenched using 3% hydrogen peroxide solution for 30 min. Sections were washed 3 times for 10 min with PBS-T and then stained using anti-IFN γ (Abcam, ab9657, 1:50), rat anti-CD3 (Abcam, ab11089, 1:250), mouse anti-NCAM (Abcam, ab9018, 1:100), goat anti-TRAIL (R&D Systems, AF375, 15 μg ml^{-1}) or anti-human GFAP-Cy3 (Sigma-Aldrich, C9205, 1:100) in blocking

buffer overnight at 4 °C. The next day slides were washed with 0.3% PBS-Tween and incubated with a mixture of donkey anti-goat Alexa Fluor 647 (Invitrogen, A21447, 1:300) and Rhodamine Red-X-AffiniPure Fab Fragment Donkey Anti-Mouse IgG (H+L) (Jackson ImmunoResearch, 715-297-003, 1:200). IFN γ was detected using Tyramide Superboost Signal Amplification kit (Thermo Fisher Scientific, B40943) according to manufacturer's instructions.

All primary antibodies were incubated overnight at 4 °C and all secondary antibodies were incubated for 2 h at room temperature. After all staining, tissues were washed 3 times for 10 min with PBS-T and 200 μ l of mounting medium with DAPI (SouthernBiotech, 0100-20) were added to the slides. Finally, tissues were covered with coverslips (VWR, 48404-111) and stored in the dark at 4 °C until imaging. Sections were imaged as described above.

Adoptive transfer of NK cells

Splenic NK cells from germ-free (GF) wild type (WT) mice, specific-pathogen free (SPF) WT mice and SPF *Irf3*^{-/-} mice were purified using NK cell-specific magnetic beads (Miltenyi, 130-115-818). Approximately 1×10^6 NK cells were adoptively transferred by intraperitoneal injection to GF WT mice and 4 days later the meninges, CNS and spleen were collected for analysis.

NK cell depletion

NK cells were depleted in naive 8-week-old C57Bl/6J mice. Anti-NK1.1 (clone PK136, BioXCell, BE0036) was injected intraperitoneally at a dose of 400 μ g in 100 μ l of 1 \times PBS per mouse. IgG2a isotype control (clone C1.18.4, BioXCell, BE0085) was administered to the control group. After 72 h CNS cells, meningeal cells, and splenic cells were isolated as described above and stained for flow cytometry. For analysis of astrocytes, CNS tissue was stained with FITC anti-mouse CD140 antibody (eBioscience, APA5, 1:100), FITC anti-mouse CD45R/B220 antibody (BD Biosciences, RA3-6B2, 1:100), FITC anti-mouse O4 antibody (R&D Systems, O4, 1:100), FITC anti-mouse TER-119 (BioLegend, TER-119, 1:100), FITC anti-mouse Ly-6G antibody (BioLegend, 1A8, 1:100), Alexa Fluor 488 anti-mouse CD105 (BioLegend, 120406, 1:100), BV570 anti-mouse Ly-6C (BioLegend, HK1.4, 1:100), BUV737 anti-mouse CD11c (BD Biosciences, HL3, 1:100), BV786 anti-mouse CD11b (BD Biosciences, M1/70, 1:100), PE-Cy5 anti-mouse CD45 (BD Biosciences, 30-F11, 1:100), PE-Cy7 anti-mouse CD253 (TRAIL) (BioLegend, N2B2, 1:100) and BUV395 anti-mouse LAMP1 (BD Biosciences, 1D4B, 1:100) for 30 min on ice. Astrocytes were gated as CD105/CD140/O4/Ter119/Ly6G/B220/Ly6C/CD3/CD11b/CD45/CD11c⁻ and LAMP1 and TRAIL expression were analysed. NK depletion was confirmed in the spleen and meninges by flow cytometry. Cells were stained with PE-Cy5 anti-mouse CD45 (BD Biosciences, 30-F11, 1:100), BV421-NK1.1 (BD Biosciences, PK136, 1:50), and BV650 or BV750-CD3 (BD Biosciences, 17A2, 1:50 and BioLegend, 100229, 1:50) for 30 min on ice. FACS was performed on a Symphony A5 (BD Biosciences).

InDrop scRNA-seq library preparation and sequencing

After flow cytometry, cells were washed in 0.1% BSA and resuspended at a concentration of 100,000 cells per ml in accordance with the InDrop workflow. InDrop runs and library

preparation were performed by the Single Cell Core Facility at Harvard Medical School. Libraries were quantified by qPCR using a Library Quantification Kit (Kapa Biosystems, KK4824) and pooled for sequencing. Libraries were sequenced on a NextSeq 500 at an average depth of 20,000–25,000 reads per cell.

InDrop scRNA-seq analysis

Filtering.—InDrop scRNA-seq data were processed using the InDrop pipeline made public on GitHub (<https://github.com/indrops/indrops>)⁷¹. We note that inDrop may capture, on average, fewer genes and unique molecular identifiers (UMIs) than other droplet microfluidic scRNA-seq technologies such as Drop-seq and 10X, potentially owing to variability between bead batches⁷² but has nevertheless been successfully used to generate many biological insights (<https://1cell-bio.com/indrop/#science>). Reads were trimmed using Trimmomatic (v.0.39) and a customized Python script which removes polyA tails (the script was integrated into the InDrop pipeline). After trimming, reads were excluded if the length of trimmed reads is less than 16 bases or if half of the bases in reads are from one single base. The reads were excluded if the UMI contained an unknown base ‘N’. The cell barcodes were filtered by two thresholds: (1) the cell barcode could not contain an N; and (2) the cell barcode must be in the cell barcode whitelist provided by the InDrop pipeline. During the mapping of cell barcode to the cell barcode whitelist, one base difference was allowed and was corrected based on the cell barcode whitelist.

Alignment and quantification.—The alignment was done using Bowtie⁷³ and the reference genome was built from EMSEMBL GRCm38.p6. Quantification was finished using the InDrop pipeline after alignment. During the quantification process the reads that were aligned to more than 10 genes were excluded, and the reads that shared one UMI while being mapped to different genes were excluded. After the quantification the cells that had less than 500 genes detected were excluded.

Integration of samples, dimensionality reductions and unsupervised

clustering of data.—The R package Seurat^{74,75} was used to analyse the dataset. Normalized counts were calculated by SCTransform software (the percentage of mitochondrial contents in each cell was regressed out during the process to prevent clustering bias owing to high mitochondrial contents cells). Next, 3,000 integration features were selected in order to integrate different samples and remove technical variability. After integration, the first 100 principal components were calculated and the first 40 are used to obtain the t-SNE plot and find neighbourhood relationships between cells. The Louvain clustering algorithm was used to perform the unsupervised clustering of the cells.

Downstream analysis.—After clustering, the model-based analysis of single cell transcriptomics (MAST) algorithm⁷⁶ was used to find differentially expressed genes in each cluster and condition. Cell type signatures were calculated using the following genes: astrocytes (*Aqp4*, *Aldh1l1*, *Gfap*, *S100b*, *Aldoc*, *Slc1a3*, *Slc1a2* and *Mfge8*); oligodendrocytes (*Mbp*, *Mag* and *Mog*); microglia (*Aif1*); neurons (*Syt1*, *Tubb3* and *Map2*). The average number of genes and UMIs detected per cell was 800 and 1,794 for the

LAMP1⁺ scRNA-seq analysis and 929 and 1,985 for the LAMP1⁺ TRAIL⁺ scRNA-seq analyses, respectively.

Drop-seq library preparation and sequencing

Drop-seq was performed as described^{16,77}. A microfluidic mask was fabricated at 125 μm in height using soft lithography. Curing agent and PDMS prepolymer (Momentive, RTV615) were mixed 1:10 and degassed in a vacuum chamber. The PDMS mixture was poured onto the master mould, further degassed, and baked at 65 °C for 4 h. The PDMS replica was punched with a 0.75-mm biopsy punch (Harris Uni-Core) and bonded to a glass slide (75 \times 50 \times 1.0 mm, Thermo Fisher Scientific, 12-550C) using a plasma bonder (Technics Plasma Etcher 500-11). The device was placed on a hot plate at 150 °C for 10 min, baked at 65 °C for 4 h, and treated with Aquapel to render it hydrophobic. A cell suspension was prepared using flow cytometry-sorted cells from mouse CNS (brain and spinal cord). Cells were counted and resuspended at 250,000 cells per ml (final concentration 125 cells per μl) in PBS and 16% Opti-prep (Sigma-Aldrich, D1556-250ML). Cell mixture was loaded into a 3 ml syringe (BD Biosciences, 309657) with a 27-gauge needle (BD Biosciences, 305109) and connected to the microfluidic device using tubing (Scientific Commodities, BB31695-PE/2). Barcoded beads (Thermo Fisher Scientific, NC0927472) were resuspended in lysis buffer consisting of: 57% Opti-prep (Sigma-Aldrich, D1556-250ML), 2.4% Ficoll PM-400 (GE Healthcare, 17-0300-10), 0.2% Sarkosyl (Teknova, S3376), 20 mM EDTA pH 8.0, 200 mM Tris-HCl pH 7.4 (Sigma-Aldrich, T2663-1L), and 50 mM DTT (Sigma-Aldrich, 646563-10X.5ML) at a concentration of 300,000 beads per ml. Beads resuspended in lysis buffer were loaded into a 3 ml syringe with a magnetic mixing disc (V&P Scientific, 772DP-N42-5-2) and gently stirred during encapsulation using a magnetic mixer (V&P Scientific, 710D2). A third syringe was loaded with oil for droplet generation (Biorad, 186-4006). To perform Drop-seq experiments, pumps were run at 1,500 $\mu\text{l h}^{-1}$ (cell mixture), 1,500 $\mu\text{l h}^{-1}$ (barcoded beads), and 4,500 $\mu\text{l h}^{-1}$ (oil) for approximately 15 min per sample. Droplets were collected, broken with 1H, 1H, 2H, 2H-perfluoro-1-octanol (PFO) (Sigma-Aldrich, 370533) added at a ratio of 1:3 PFO:oil, washed with 10 ml 6 \times SSC (National Diagnostics, EC-873), and centrifuged for 1 min at 1,000g. Beads at the interface were removed, oil was eliminated, and beads were washed 3 times with 6 \times SSC. Beads were next washed with Maxima H-minus 1 \times reverse transcription (RT) buffer (Thermo Fisher Scientific, EP0753). Beads were resuspended in 50 μl of Maxima H-minus 1 \times RT buffer. The following RT mixture was added to each tube of beads: 40 μl 20% Ficoll PM-400, 30 μl 5 \times Maxima H-minus RT buffer, 2 μl 100 mM dNTPs (Life Technology, 4368813), 5 μl 100 μM template switching oligonucleotide (TSO) primer (IDT), 5 μl RNase inhibitor (Lucigen, 30281-2), 58 μl nuclease free water, and 10 μl Maxima H-minus reverse transcriptase (Thermo Fisher Scientific, EP0753). Beads suspended in RT mixture were incubated at room temperature for 30 min on an inverter, followed by 90 min at 42 °C on an inverter. Following reverse transcription, beads were washed once with 1 ml TE-SDS (10 mM Tris-HCl pH 8.0, 1 mM EDTA pH 8.0, 0.5% SDS), and twice with TE-TW (10 mM Tris-HCl pH 8.0, 1 mM EDTA pH 8.0, 0.01% Tween-20) and pelleted during each step by centrifuging at 1,000g for 1 min. Beads were washed once with 10 mM Tris-HCl pH 8.0 and resuspended in exonuclease mix consisting of: 170 μl nuclease free water, 20 μl 10 \times Exonuclease I buffer, and 10 μl Exonuclease I (Thermo Fisher Scientific, EN0582). Resuspended beads were incubated for

45 min at 37 °C with inversion. After treatment, beads were washed once with TE-SDS, twice with TE-TW, and twice with nuclease free water. Beads were counted and resuspended at a concentration of 80 beads per μl in preparation for PCR. Beads were then added to a PCR tube at a concentration of 2,000 beads per tube. PCR mix (25 μl HiFi Hot-Start ReadyMix (Kapa Biosystems, KK2602); 0.4 μl 100 μM SMART PCR primer (IDT)) was added to each tube and beads were manually mixed before PCR. PCR cycling conditions were: 95 °C (3 min.); 4 cycles of: 98 °C (20 s), 65 °C (45 s), 72 °C (3 min); 9 cycles of: 98 °C (20 s), 67 °C (20 s), 72 °C (3 min); 72 °C (5 min); 4 °C hold. Following PCR, cDNA samples were purified in a 96-well plate (Biorad, HSP9611) on a magnetic stand (NEB, S1511S) using Agencourt AMPure XP magnetic beads (Beckman Coulter, A63881) at a 0.6 \times ratio according to the standard protocol. The sample from each PCR tube was eluted in 10 μl nuclease free water, and technical replicates were pooled following elution. cDNA was run on a Bioanalyzer High Sensitivity DNA chip (Agilent Technologies, 5067-4626) on a 2100 Bioanalyzer (Agilent). For cDNA library tagmentation, 600 pg of cDNA in 5 μl was added to 10 μl of Nextera Tagment DNA buffer and 5 μl of Amplicon Tagment Mix (Illumina, FC-131-1096). cDNA was tagmented at 55 °C for 5 min, followed by addition of room temperature-equilibrated 5 μl Neutralize Tagment buffer (Illumina, FC-131-1096). Samples sat at room temperature for 5 min followed by addition of 15 μl Nextera PCR Mix (Illumina, FC-131-1096), 8 μl nuclease free H₂O, 1 μl 10 μM New-P5-SMART PCR hybrid oligo (IDT), and 1 μl of 10 μM Nextera indexing oligonucleotide (Invitrogen). Samples were PCRred using the following conditions: 95 °C (30 s); 12 cycles of: 95 °C (10 s), 55 °C (30 s), 72 °C (30 s); 72 °C (5 min); 4 °C hold. Tagmented libraries were purified using Agencourt AMPure XP magnetic beads at a 0.6 \times ratio according to the manufacturer's protocol and eluted in 10 μl nuclease free H₂O. Samples were then run on a Bioanalyzer 2100 to assess library size. Libraries were quantified by qPCR using a Library Quantification Kit (Kapa Biosystems, KK4824). Tagmented libraries were pooled at 5 nM concentration and sequenced using a NovaSeq S1 at the Broad Institute using a Custom Read 1 primer and 20 + 80 bp reads.

Drop-seq analysis

Trim Galore (v.0.6.0) was used to trim the adaptor contents and the 5' primers. Single-cell paired-end reads were then processed using Drop-seq software (v.2.0.0)⁷⁷. After associating every read with its associated cell barcode and UMIs, read alignment was performed using STAR software (2.5.2) to mouse reference genome, which was prepared from the ENSEMBL Mouse Genome (GRCm38.p6). After alignment, bam files were sorted using Picard software, and bead synthesis errors (indels or substitutions) were detected and fixed by using Drop-Seq software. After fixing bead synthesis errors, gene expression was quantified using Drop-Seq software, using the parameter of 'min_num_genes_per_cell = 500.' Using Seurat^{74,75}, expression matrices of samples were log-normalized and doublets removed. Canonical correlation analysis⁷⁴ was performed to correct for batch effects and to integrate different samples within each dataset. After the integration of different samples within each dataset, principal component analysis was performed to determine the number of principal components (PCs) to use during the dimension reduction and clustering analysis. The first 50 PCs were used. To cluster cells, the Louvain algorithm was applied to the integrated datasets with a resolution parameter of 0.5. After clustering, the MAST

algorithm⁷⁶ was used to conduct differential expression analysis for each cluster compared to all other cells. The results of the differential expression analysis were used in further downstream analysis. Visualization was performed using t-SNE^{78,79}. Cells were characterized by the following parameters: 1,727 UMIs per cell, 814 genes per cell, and 173,000 reads per cell per sample.

RNAscope analysis

Mice were intracardially perfused with ice cold 1× PBS followed by ice cold 4% PFA. Spinal columns were then transferred to 20% EDTA pH 7.4 (Thermo Fisher Scientific, S28291GAL) at 4 °C with inversion until bone was decalcified. Samples were then dehydrated in 30% sucrose for 2 days at 4 °C. Spinal cords from naive or EAE mice were frozen in OCT (Sakura, 4583) and stored at –80 °C. 15-µm sections were collected on SuperFrost Plus slides (Thermo Fisher Scientific, 22-037-246) using a cryostat and baked at 60 °C for 30 min then stored at –80 °C. Slides were removed from the freezer and thawed to room temperature, then baked 60 °C for 30 min, rinsed in reverse osmosis (RO) water, baked again on a slide warmer for 15 min and finally dipped in 100% EtOH to ensure tissue adherence to the slides. RNAscope protocol was adapted from the Advanced Cell Diagnostics user manual using all ACD provided reagents. Endogenous peroxide activity of samples was quenched with H₂O₂ solution (ACD, 322381) on the slides for 10 min at room temperature. Slides were then rinsed in RO water, dried on the slide dryer, and dipped in 100% EtOH. Target retrieval was performed by submerging slides in Target Retrieval reagent (ACD, 322000) at 90–95 °C for 5 min on a hotplate. Samples were rinsed in RO water, dried on the slide dryer, and dipped in 100% EtOH. At this point, a hydrophobic barrier was drawn on the slides around the tissue sections (ACD, ImmEdge Hydrophobic Barrier Pen, 310018). After target retrieval, tissue was further permeabilized using Protease Plus (ACD, 322381) for 30 min in the HybEZ II humidity controlled hybridization oven (ACD, 321710/321720) at 40 °C and then washed twice in RO. RNA 3-plex probe hybridization (ACD, *Ifng*-C1 311391, *Tnfsf10*-C2 500111-C2, *Gfap*-C3 313211-C3) was performed in the HybEZ oven for 2 h at 40 °C. Slides were washed twice in Wash Buffer (ACD, 310091) and stored overnight at room temperature in 5× SSC. The next day, slides were washed twice in Wash Buffer. Hereafter, samples were washed twice in Wash Buffer reagent following each subsequent step. RNA probes were next amplified and detected on the slides using the RNAscope Multiplex Fluorescent Detection Kit v2 (ACD, 323110) according to the manufacturer's protocol. Specifically, samples were incubated in Amp1, Amp2, and Amp3 sequentially for 30 min, 30 min, and 15 min, respectively at 40 °C in the HybEZ oven. The channel 1 probe (*Ifng*) was developed by first conjugating the HRP using HRP-C1 for 15 min at 40 °C in the HybEZ oven, then incubating in the Opal570 fluorophore (Akoya Biosciences, FP1487001KT) diluted to 1:1,000 in TSA buffer (ACD, 322809) for 30 min at 40 °C in the HybEZ oven, and finally blocking using the HRP-Blocking reagent for 15 min at 40 °C in the HybEZ oven. The channel 2 probe (*Tnfsf10*) was developed by conjugating the HRP using HRP-C2 for 15 min at 40 °C in the HybEZ oven, then incubating in the Opal520 fluorophore (Akoya Biosciences, FP1488001KT) diluted to 1:750 in TSA buffer for 30 min at 40 °C in the HybEZ oven, and finally blocking using the HRP-Blocking reagent for 15 min at 40 °C in the HybEZ oven. The channel 3 probe (*Gfap*) was developed by conjugating the HRP using HRP-C3 for 15 min at 40 °C in the HybEZ oven, then

incubating in the Opal690 fluorophore (Akoya Biosciences, FP1497001KT) diluted to 1:1,000 in TSA buffer for 30 min at 40 °C in the HybEZ oven, and finally blocking using the HRP-Blocking reagent for 15 min at 40 °C in the HybEZ oven. Slides were washed a final time in Wash Buffer before proceeding to astrocyte immunofluorescence. Slides were blocked in SuperBlock (Thermo Fisher Scientific, 37515) overnight at 4 °C in the dark. The next day, tissue was incubated in primary mouse anti-GFAP (Millipore, MAB360, 1:500) for 1 h in the HybEZ oven at 40 °C. After incubation, slides were washed twice in TBS followed by detection with Alexa Fluor 700 (Thermo Fisher Scientific, A-21036, 1:300) for 1 h in the HybEZ oven at 40 °C. Tissues were washed twice in TBS and incubated with DAPI (included in ACD detection kit) for 30 s and then coverslipped using ProLong Gold (Thermo Fisher Scientific, P10144) mounting medium. *Gfap* was stained with the Opal570 fluorophore (1:1500) for analysis of its co-localization with anti-GFAP antibody staining, which was stained using Alexa Fluor 700. For *Klrb1c/Tnfsf10* detection, the RNAscope protocol was performed as above. The channel 2 probe (*Tnfsf10*) was conjugated to the Opal520 fluorophore diluted to 1:750 in TSA buffer and the channel 3 probe (*Klrb1c*) was conjugated to the Opal570 fluorophore diluted to 1:1,000 in TSA buffer. GFAP immunofluorescence was performed as described above. All sections were left to dry overnight in the dark at 4 °C until imaging. Images were acquired using a Zeiss LSM 710 NLO confocal microscope equipped with a motorized stage, four lasers and an acquisition camera.

Bulk RNA-seq

Sorted cells were lysed and RNA isolated using the Qiagen RNeasy Micro kit (Qiagen, 74004) with on-column DNase I digestion (Qiagen, 79254). RNA was concentrated with a Savant Speedvac Concentrator (Thermo Fisher Scientific, DNA120) when needed. RNA was suspended in 5 μ l of nuclease free water at a concentration of 0.5-1 ng μ l⁻¹ and sequenced using or SMARTSeq2⁸⁰ at the Broad Institute. All bulk RNA-sequencing results were aligned to EMSEMBL GRCm38.p6 reference genome and quantified using Kallisto (v.0.46.1)⁸¹ and Salmon (v.1.1.0)⁸². DESeq2 software was used to perform differential expression analysis and the apeGLM algorithm⁸³ was used to remove noise in log₂ fold change analyses following differential expression analysis.

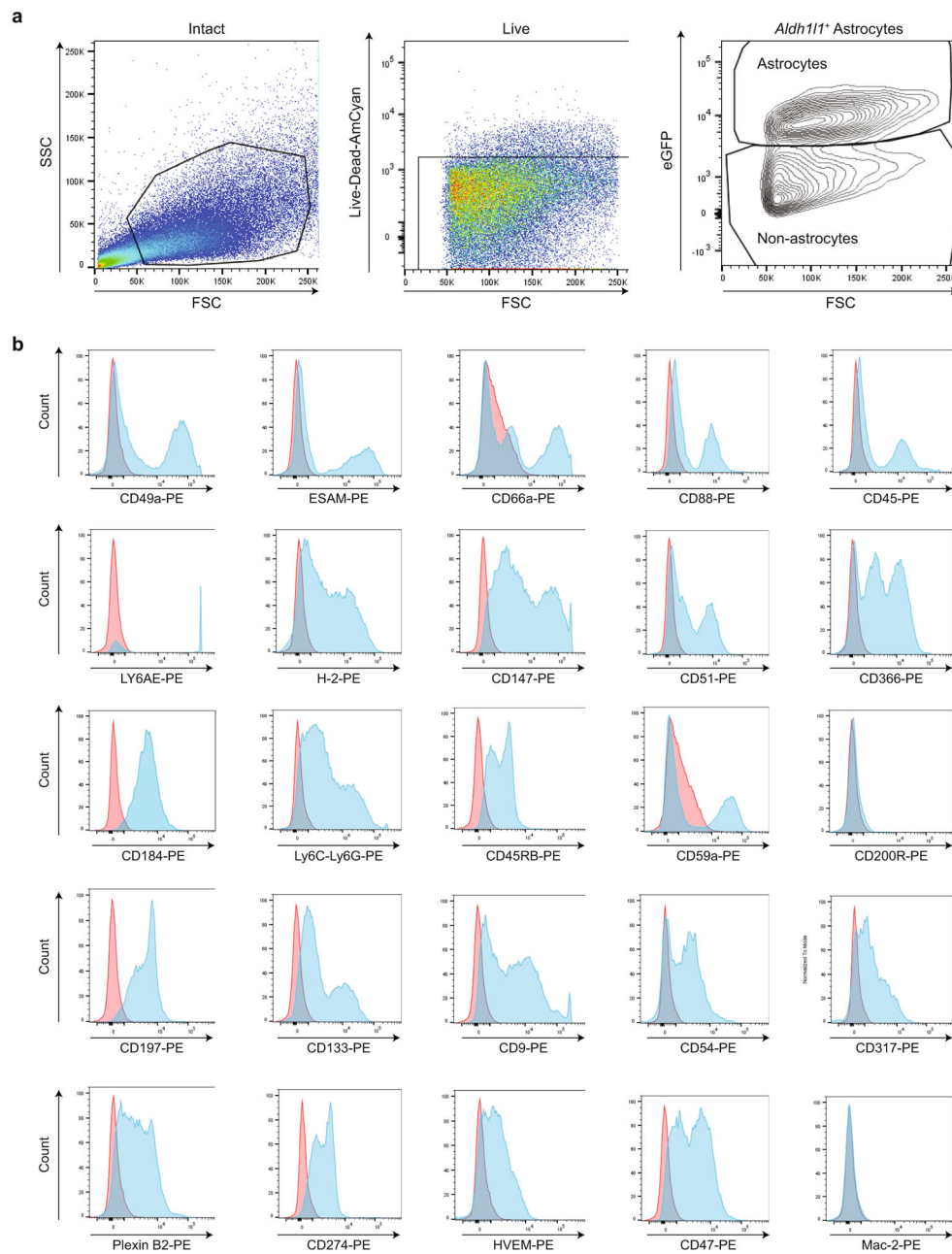
Pathway analysis

GSEA or GSEAPreranked analyses were used to generate enrichment plots for bulk RNA-seq or scRNA-seq data^{84,85} using MSigDB molecular signatures for canonical pathways: KEGG/Reactome/Biocarta (c2. cp.all), Motif (c3.all), Gene ontology (c5.cp.all), and Hallmark (h.all). Alternatively, ENRICHR^{86,87} was used when a list of differentially expressed genes by group was calculated to identify overrepresented transcriptional motifs or pathways. Protein class identity was classified using PantherDB⁸⁸. To determine regulators of gene expression networks, Ingenuity Pathway Analysis software (Qiagen) was used by inputting gene expression datasets with corresponding log (FoldChange) expression levels compared to other groups. “Canonical pathways” and “upstream analysis” metrics were considered significant at $P < 0.05$.

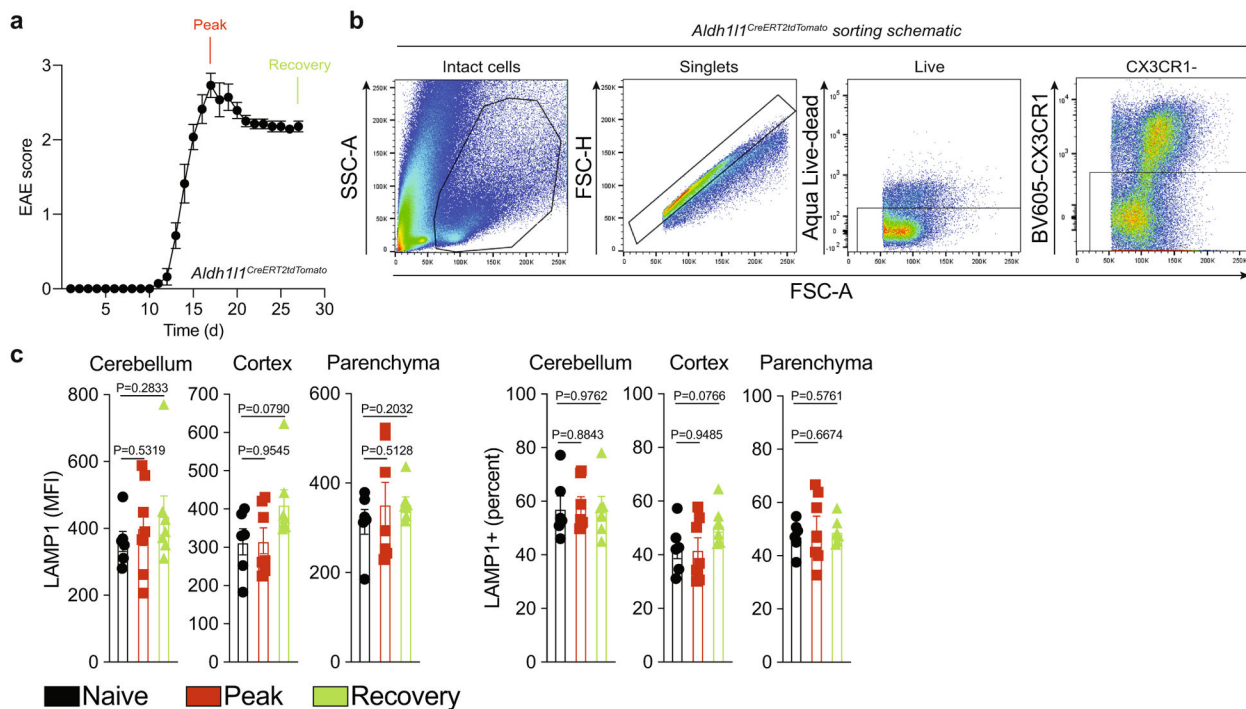
Reporting summary

Further information on research design is available in the Nature Research Reporting Summary linked to this paper.

Extended Data

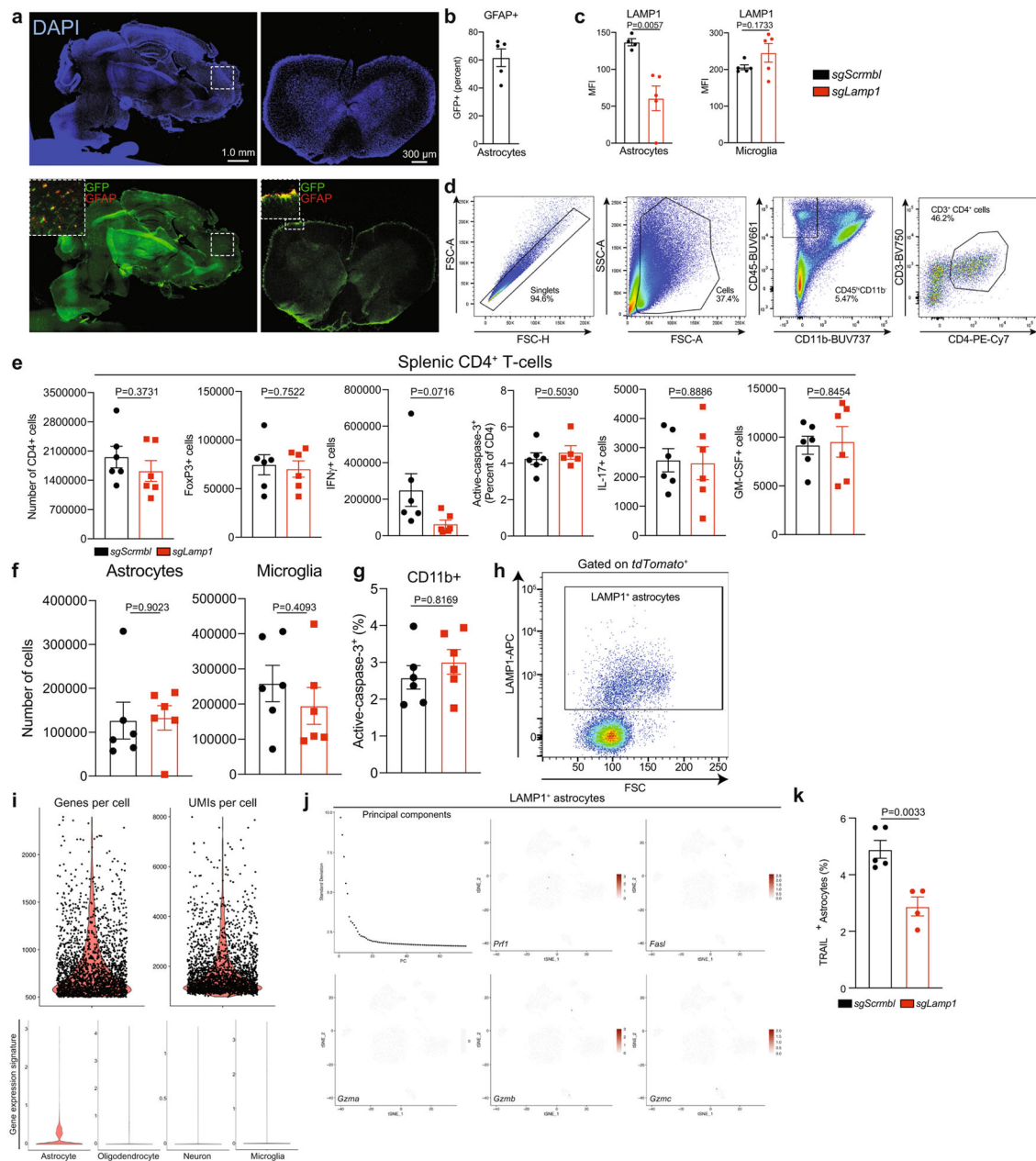


Extended Data Fig. 1 | Profiling of astrocyte surface markers.
a, Sample FACS gating strategy. **b**, Histogram depicting the expression of surface markers in astrocytes.



Extended Data Fig. 21. Analysis of differentially expressed astrocyte surface markers.

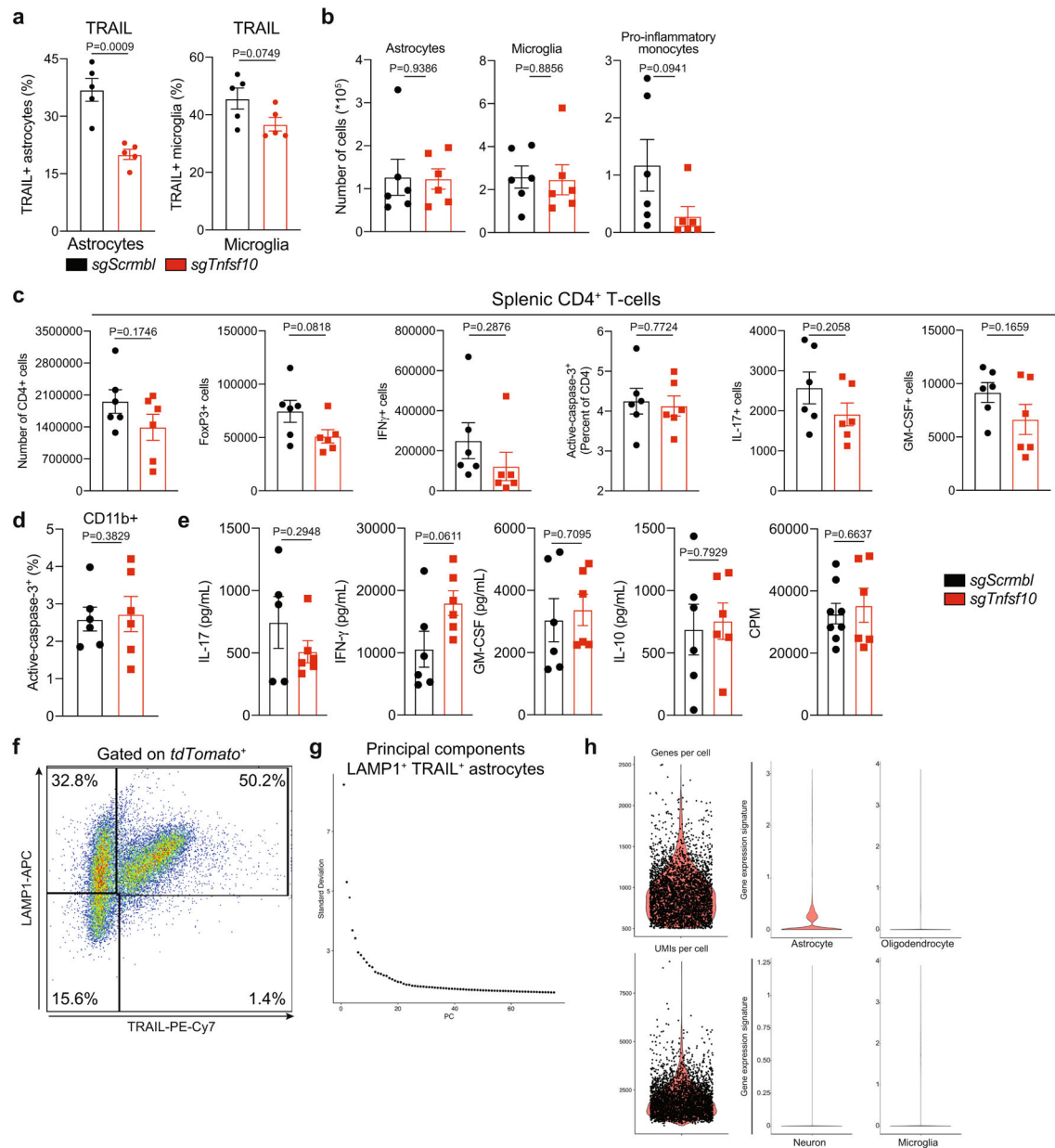
a, EAE in *Aldh111^{CreERT2}tdTomato* mice. $n = 6$ naive, $n = 7$ peak, $n = 7$ recovery mice. **b**, Sorting schematic for tdTomato⁺ astrocytes. **c**, MFI of LAMP1 expression from screening. $n = 6$ naive, $n = 7$ peak, $n = 7$ recovery mice. Unpaired two-tailed t -test. Data are mean \pm s.e.m.



Extended Data Fig. 3 l. Analysis of LAMP1⁺ astrocytes.

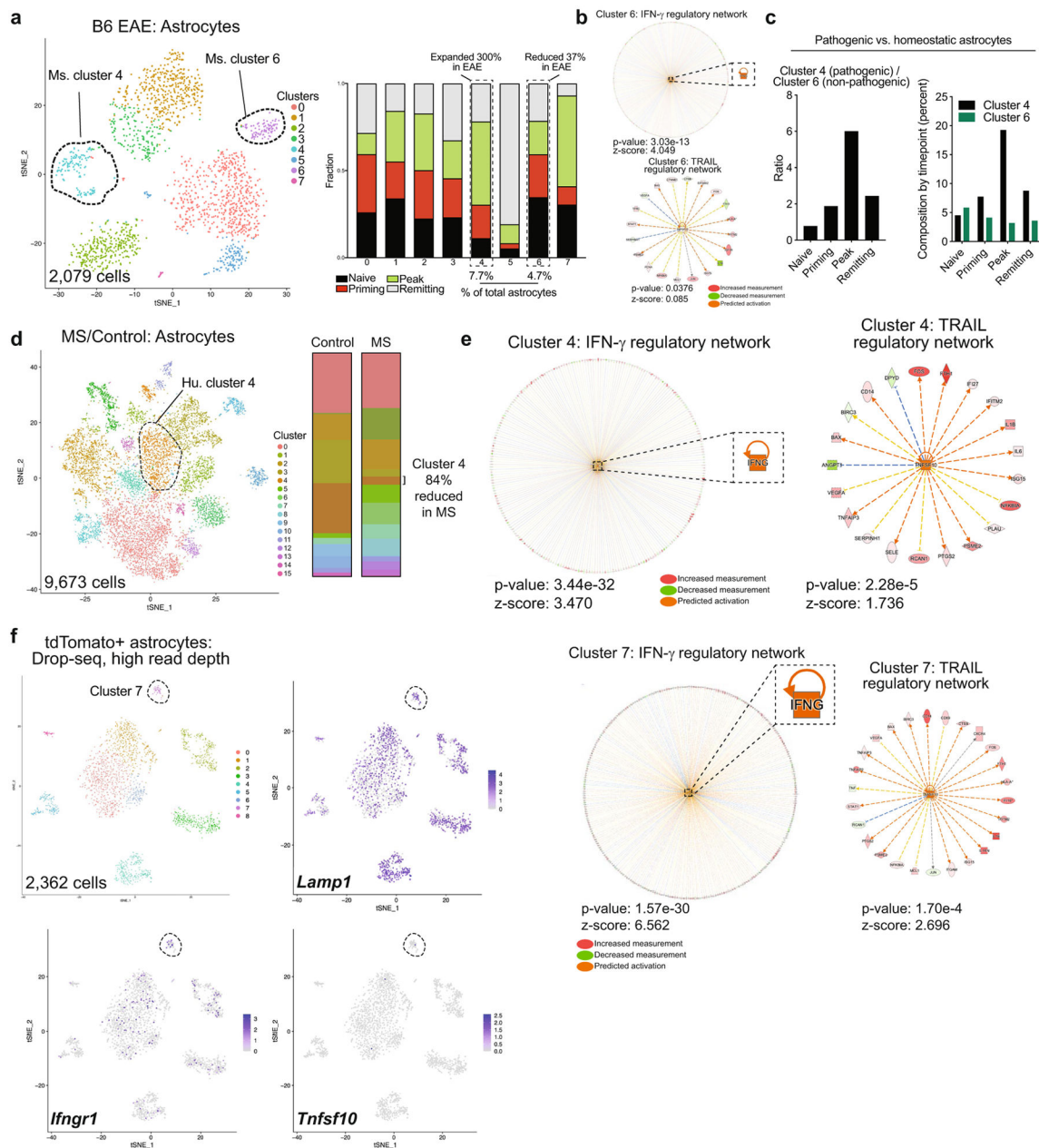
a, Immunostaining of brain and spinal cord of mice transduced with *Gfap*-driven Cas9-2A-EGFP lentivirus. Representative images from $n = 5$ mice analysed. **b**, Percentage of GFP⁺GFAP⁺ cells by FACS. $n = 5$ mice. **c**, Quantification of astrocyte LAMP1 knockdown in astrocytes and microglia by FACS. $n = 4$ mice (sgScramble astrocyte); $n = 5$ mice otherwise. Unpaired two-tailed *t*-test. **d**, Gating strategy of CD4⁺ T cells from CNS. **e**, Analysis of splenic T cells from sgScramble- or sgLamp1-transduced mice. $n = 5$ mice sgLamp1 active-caspase 3; $n = 6$ mice otherwise. Unpaired two-tailed *t*-test. **f**, Analysis of CNS cells isolated from sgScramble- or sgLamp1-transduced mice. $n = 6$ per group. Unpaired two-tailed *t*-test. **g**, Analysis of CD11b⁺ cell apoptosis in sgScramble- or sgLamp1-transduced mice. $n = 6$

per group. Unpaired two-tailed *t*-test. **h**, Example gating used to sort LAMP1⁺ astrocytes from *Aldh111^{creERT2}tdTomato* mice for scRNA-seq. **i**, Violin plots of genes, UMIs and cell-type markers for cells analysed by scRNA-seq from naive and EAE mice 17 days after induction. Astrocyte markers include *Aqp4*, *Aldh111*, *Gfap*, *S100b*, *Aldoc*, *Slc1a3*, *Slc1a2* and *Mfge8*. **j**, Principal components used and gene expression scatterplots of LAMP1⁺ astrocytes isolated from *Aldh111^{creERT2}tdTomato* mice. **k**, TRAIL expression on astrocytes from sgScramble- and sgLamp1-transduced mice 28 days after EAE induction. *n* = 5 sgScramble, *n* = 4 sgLamp1 mice. Unpaired two-tailed *t*-test. Data are mean ± s.e.m.



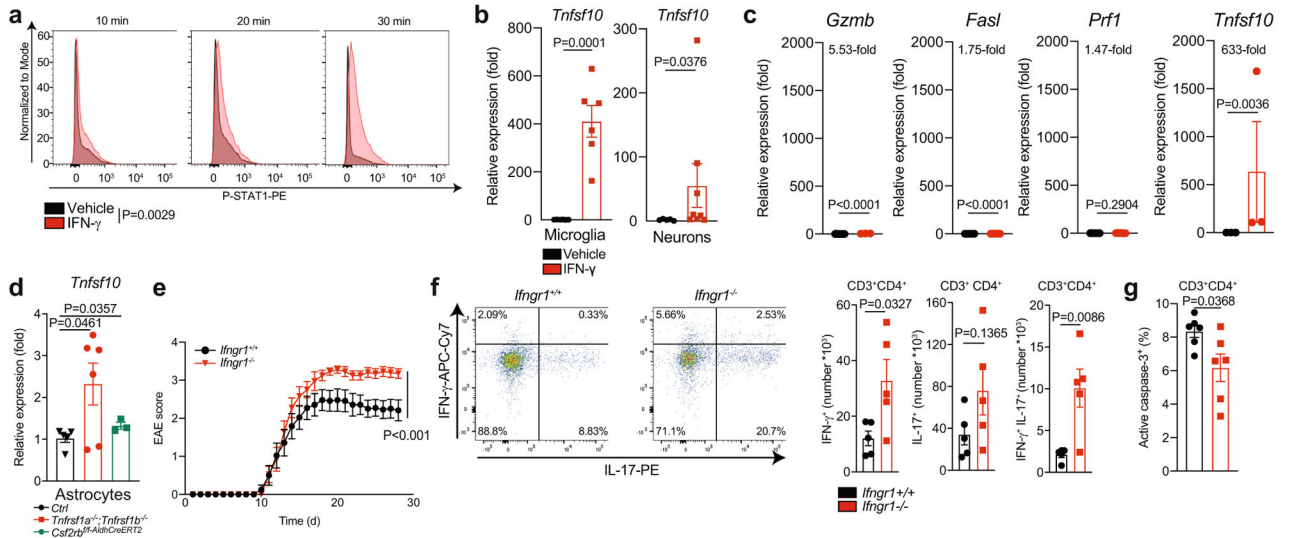
Extended Data Fig. 4 l. Analysis of TRAIL⁺ astrocytes.

a, Quantification of TRAIL knockdown using FACS in astrocytes and microglia. $n = 5$ mice per group. Unpaired two-tailed t -test. **b**, Analysis of CNS cell numbers in sgScramble- or sgTnfsf10-transduced mice. $n = 6$ mice per group. Unpaired two-tailed t -test. **c**, Control analyses of splenic T cells from knockdown mice. $n = 6$ mice per group. Unpaired two-tailed t -test. **d**, Analysis of CD11b⁺ cell apoptosis in sgScramble- or sgTnfsf10-transduced mice. $n = 6$ mice per group. Unpaired two-tailed t -test. **e**, Cytokine production and recall response of splenic T cells isolated from knockdown mice. $n = 6$ mice per group. $n = 8$ sgScramble CPM, $n = 5$ sgScramble IL-17 mice. Unpaired two-tailed t -test. **f**, Sorting schematic of LAMP1⁺TRAIL⁺ astrocytes from *Aldh111^{creERT2tdTomato}* mice for scRNA-seq. **g**, Principal components used in scRNA-seq analysis of LAMP1⁺TRAIL⁺ astrocytes isolated from *Aldh111^{creERT2tdTomato}* mice from naive and EAE mice at 17 days after induction. **h**, Violin plots of genes, UMIs and cell-type markers for cells analysed. Astrocyte markers include *Aqp4*, *Aldh111*, *Gfap*, *S100b*, *Aldoc*, *Slc1a3*, *Slc1a2* and *Mfge8*. Data are mean \pm s.e.m.



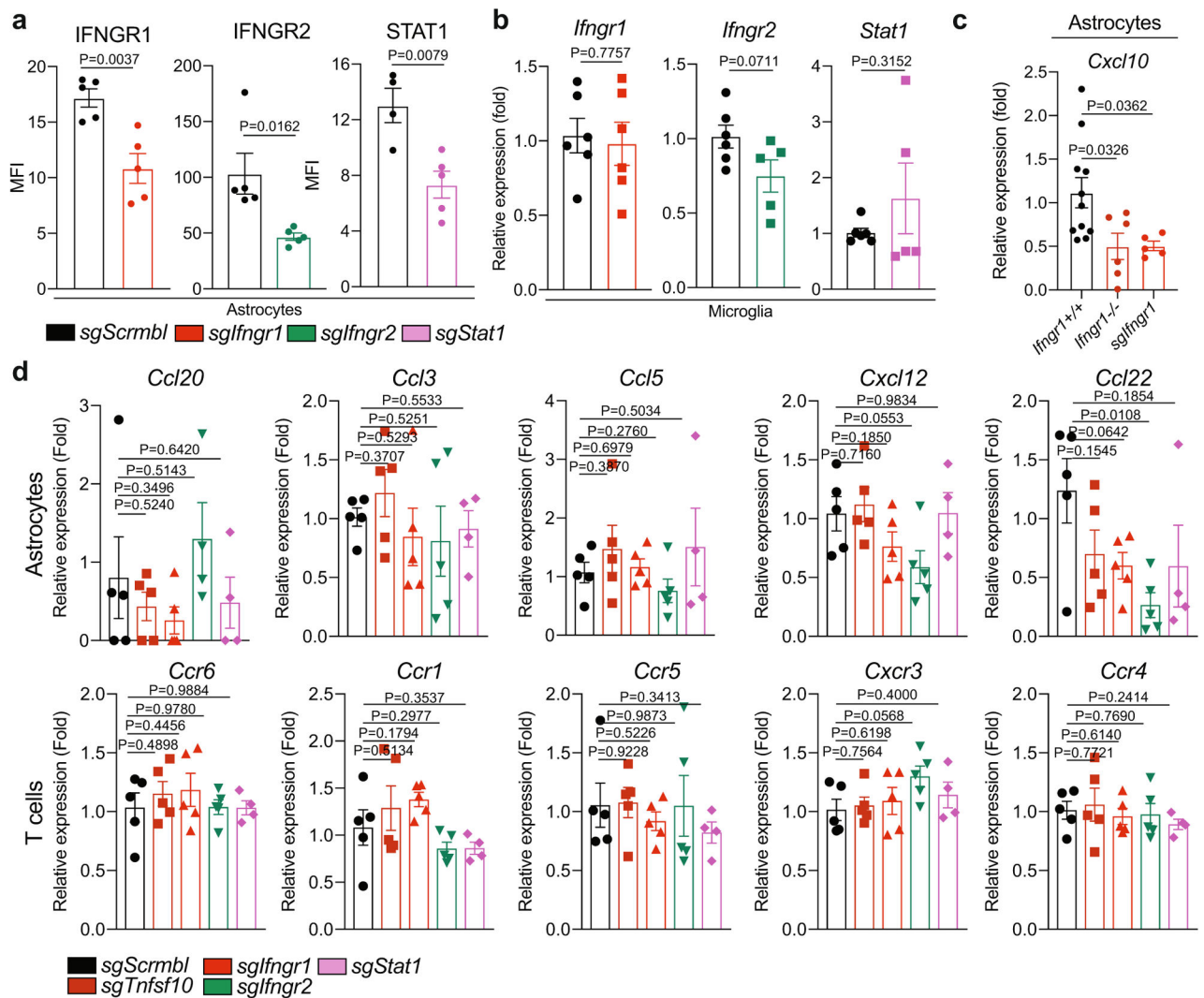
Extended Data Fig. 5 l. IFN γ -TRAIL signalling in other datasets.

a, b, Identification of an IFN γ -TRAIL signalling network in a population of mouse astrocytes (cluster 6) previously analysed during the course of EAE in a previous study¹⁶. **c**, Comparison of the relative abundance of homeostatic vs pathogenic glia over the course of EAE. Compared to a pathogenic astrocyte population, astrocytes regulated by IFN γ and characterized by TRAIL are de-enriched during EAE. **d, e**, Identification of an IFN γ -TRAIL signalling network in a patient with MS or control astrocytes previously analysed by scRNA-seq during MS in a previous study¹⁶. $n = 25$ mice. $n = 48$ humans. **f**, Analysis by Drop-seq of tdTomato+ astrocytes isolated by flow cytometry. Data shown as mean \pm s.e.m.



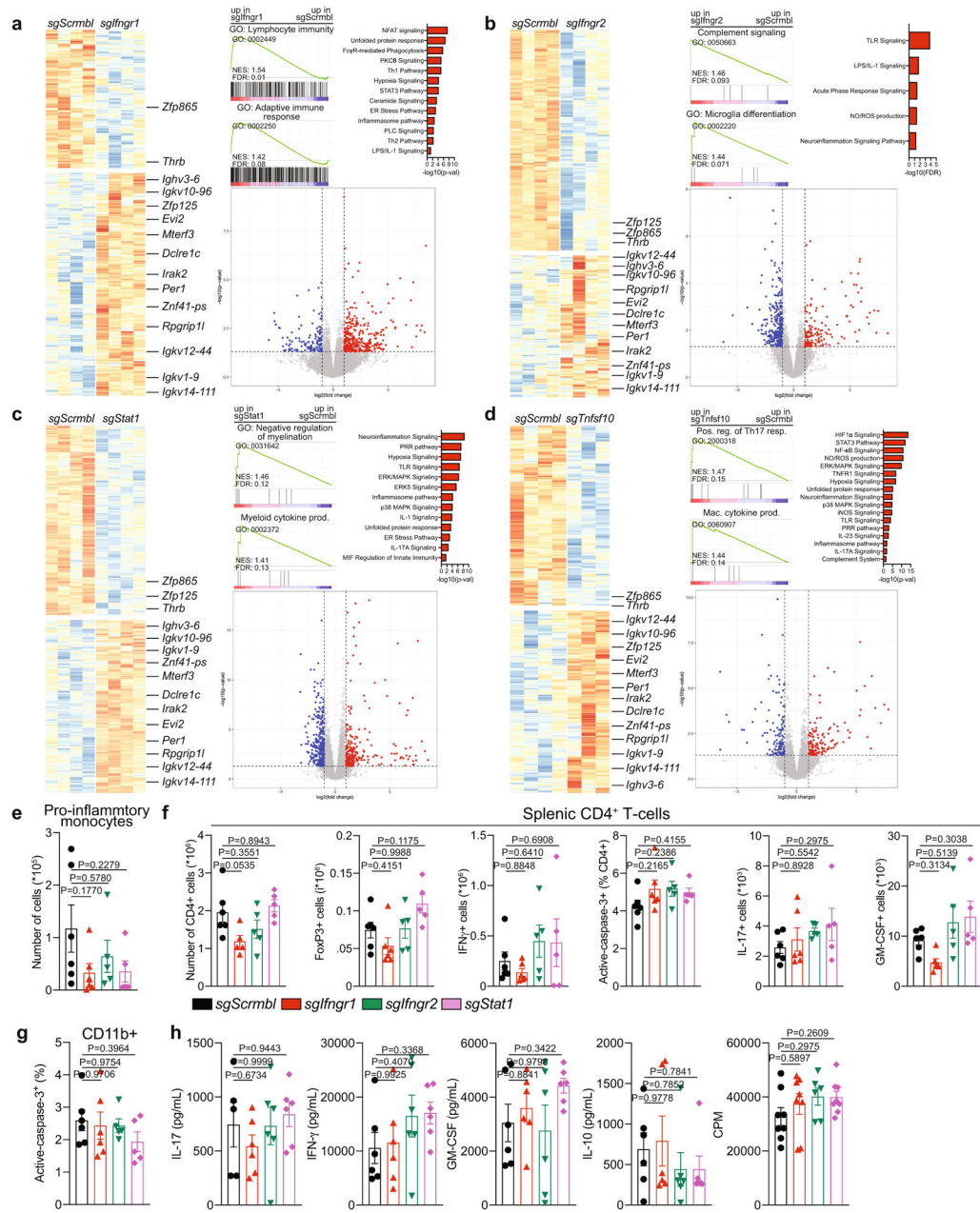
Extended Data Fig. 6 l. IFN γ signalling in LAMP1⁺TRAIL⁺ astrocytes.

a. STAT1 phosphorylation determined by flow cytometry in mouse astrocytes in culture treated with IFN γ or vehicle. $n = 4$ per condition. Unpaired two-tailed t -test. Experiment repeated three times. **b.** Analysis of *Tnfsf10* expression in primary microglia and neurons in response to IFN γ . $n = 8$ for neuron IFN γ -treated, $n = 5$ neuron veh, $n = 6$ otherwise. Unpaired two-tailed t -test, data log-normalized for neuron *Tnfsf10*. **c.** Analysis of other apoptosis-promoting molecules expressed by astrocytes. $n = 14$ *Fasf* vehicle; $n = 13$ *Gzmb* vehicle; $n = 12$ *Prf1* vehicle.; $n = 7$ *Fasf* IFN γ ; $n = 7$ *Prf1* IFN γ ; $n = 3$ *Gzmb* IFN γ ; $n = 3$ for *Tnfsf10*. Unpaired two-tailed t -test. *Tnfsf10* data *In*-transformed. Note the consistent axis scale. **d.** Analysis of *Tnfsf10* expression by qPCR in astrocytes isolated from mice null for the indicated genes 29 days after EAE induction. $n = 5$ Ctrl, $n = 3$ *csf2rb*^{f/f}-*Aldh11creERT2*, $n = 6$ *Tnfrsf1a*^{-/-};*Tnfrsf1b*^{-/-} mice. Unpaired two-tailed t -test (*Tnfrsf1a*^{-/-};*Tnfrsf1b*^{-/-}) and Mann-Whitney test (*Csf2rb*^{f/f}-*Aldh11creERT2*). **e.** EAE in *Ifngr1*^{+/+} ($n = 12$ mice) or *Ifngr1*^{-/-} ($n = 10$ mice). Two-way repeated measures ANOVA. **f.** Flow cytometry analysis of T cells in the CNS of *Ifngr1*^{+/+} or *Ifngr1*^{-/-} mice. $n = 5$ mice per group. Unpaired two-tailed t -test. **g.** Caspase-3 activation in CD4⁺ T cells isolated from the CNS of *Ifngr1*^{+/+} or *Ifngr1*^{-/-} mice. $n = 6$ per group. Unpaired two-tailed t -test. Data are mean \pm s.e.m.



Extended Data Fig. 7 l. Effects of astrocyte-specific knockdown of IFN γ signalling.

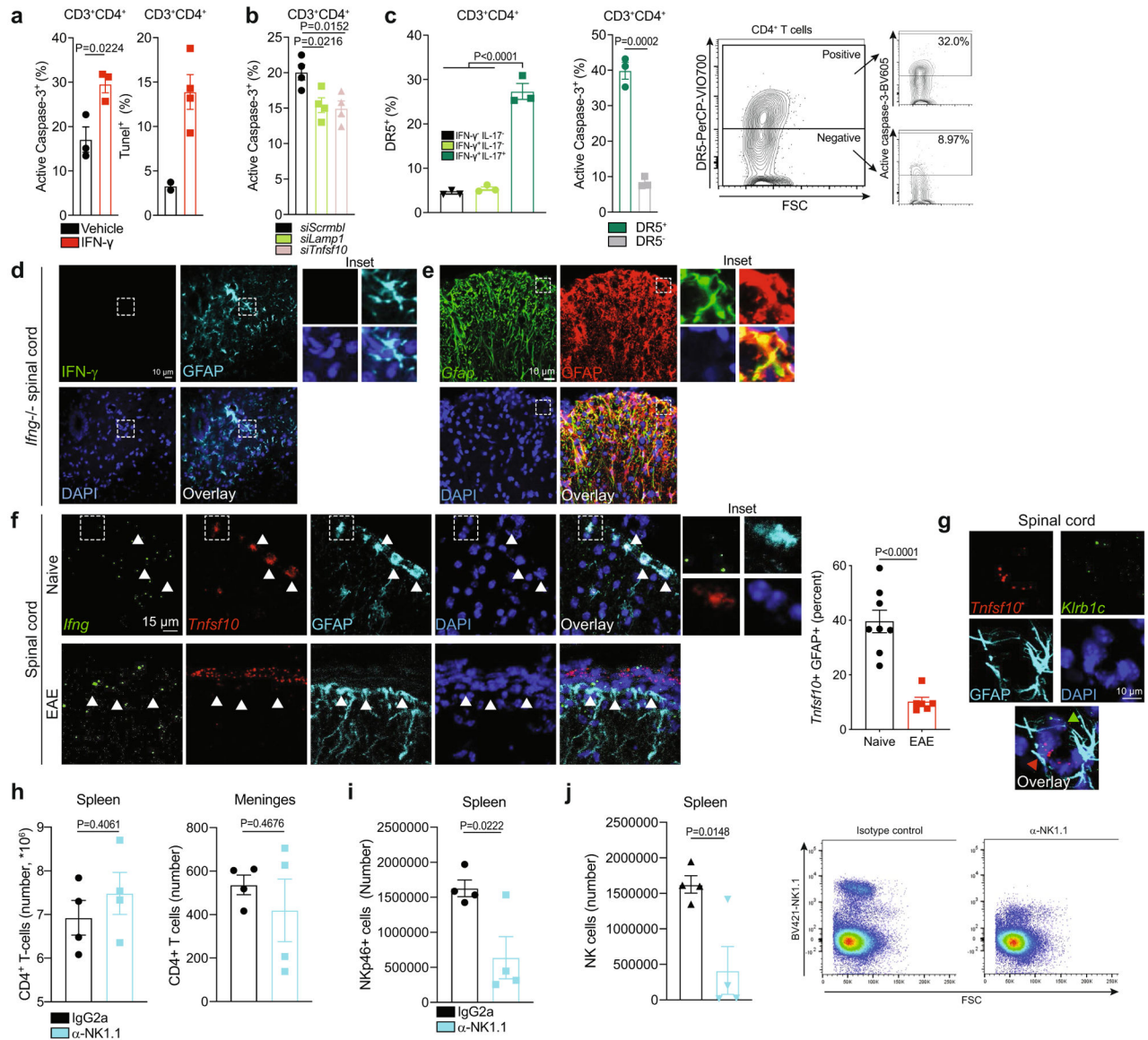
a, Knockdown analyses by FACS of mice transduced with *sgScramble*, *sgIfngr1*, *sgIfngr2* and *sgStat1*. $n = 5$ mice per group. $n = 4$ *sgScramble* *STAT1* mice. Unpaired two-tailed t -test. **b**, Control analyses of microglial expression following astrocyte knockdown. $n = 5$ *sgIfngr2*, $n = 5$ *sgStat1*, $n = 6$ mice otherwise. Unpaired two-tailed t -test. **c**, Analysis of *Cxcl10* expression in astrocytes isolated from *Ifngr1*^{+/+}, *Ifngr1*^{-/-} or *sgIfngr1* mice 29 days after EAE induction. $n = 11$ *Ifngr1*^{+/+}, $n = 6$ *Ifngr1*^{-/-}, $n = 5$ *sgIfngr1*. Unpaired two-tailed t -test. **d**, Analysis of astrocyte chemokine and T cell chemokine receptor expression from knockdown mice 29 days after EAE induction. $n = 4$ *sgStat1*, $n = 4$ *sgIfngr2* *Ccl20*, $n = 5$ mice otherwise. Unpaired two-tailed t -test per condition. Data are mean \pm s.e.m.



Extended Data Fig. 8. Microglia monocyte, and peripheral T cell responses to astrocyte perturbation.

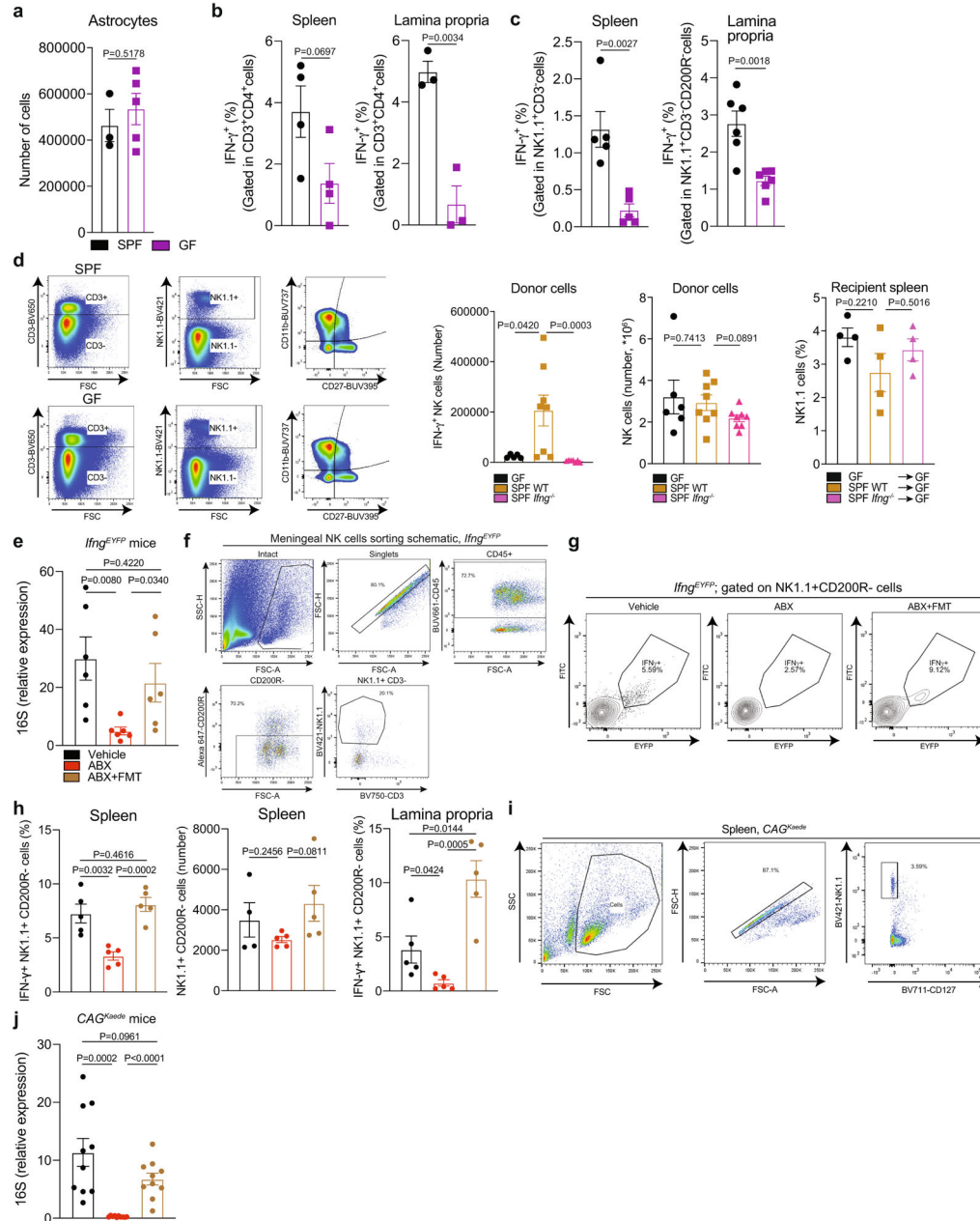
a–d, Bulk RNA-seq analyses of microglia (CD11b⁺CD45⁺Ly6C^{low}) isolated by flow cytometry from mice transduced with the indicated astrocyte-targeting CRISPR–Cas9 lentivirus 24 days after EAE induction. Heat map of differentially expressed genes, GSEA analysis, Qiagen IPA and volcano plot shown per group. n = 4 mice per group, n = 3 mice for *sgTnfsf10*. e, Control analyses of CNS-recruited pro-inflammatory monocytes. n = 6 *sgScramble*, *sgIfngr1*; n = 5 mice otherwise. One-way ANOVA, Sidak post-hoc test. f, Control analyses of splenic T cells. n = 6 *sgScramble*, *sgIfngr1*; n = 5 *sgIfngr1* CD4⁺, n = 5 mice otherwise. One-way ANOVA, Dunnett post-hoc test. g, Analysis of active-caspase 3

expression in CD11b⁺ cells. $n = 6$ sgScramble, sgIfngr1; $n = 5$ mice otherwise. One-way ANOVA, Dunnett post-hoc test. **h**, Cytokine production and recall response of splenic T cells isolated from knockdown mice. $n = 6$ per group. $n = 5$ sgScramble IL-17, $n = 8$ sgScramble, sgIfngr1, sgStat1 CPM mice. One-way ANOVA, Dunnett post-hoc test. Data are mean \pm s.e.m.



Extended Data Fig. 9 l. Control analyses of in vitro apoptosis and anti-NK1.1 antibody depletion.
a, Active caspase-3 and TUNEL FACS analysis In CD4⁺ T cells co-cultured with astrocytes pre-treated with vehicle or IFN γ . $n = 3$ for active-caspase 3, $n = 2$ for TUNEL vehicle, $n = 4$ for TUNEL IFN γ . Unpaired two-tailed t -test. **b**, Active caspase-3 expression in CD4⁺ T cells co-cultured with astrocytes transfected with the indicated siRNA. $n = 4$ per condition. Unpaired two-tailed t -test. **c**, Left, DR5 expression in cultured IFN γ ⁺, IFN γ ⁺IL-17⁺ and IFN γ ⁻IL-17⁻ CD4⁺ T cells activated in vitro. $n = 3$ per group. One-way ANOVA, Dunnett

post-hoc test. Right, active-caspase 3 expression in DR5⁺ or DR5⁻ CD4⁺ T cells co-cultured with IFN γ -pre-treated astrocytes. $n = 3$ per group. Unpaired two-tailed t -test. **d**, Negative control images of IFN γ immunostaining using *Ifng*^{-/-} mice. Repeated twice. **e**, Fluorescent in situ hybridization (FISH) of *Gfap* co-stained with anti-GFAP antibody. Repeated three times. **f**, FISH of *Tnfsf10* and *Ifng* in naive or EAE mouse spinal cord co-stained with anti-GFAP antibody. $n = 8$ images (naive), $n = 6$ images (EAE). Unpaired two-tailed t -test. Repeated three times. **g**, FISH of *Ifng*, *Tnfsf10*, and *Klrb1c* in naive or EAE mouse spinal cord. Green arrowhead, NK cell; red arrowhead, astrocyte. Repeated twice. **h**, Control analyses for anti-NK1.1 antibody depletion experiment. $n = 4$ per group. Unpaired two-tailed t -test. **i**, Quantification of splenic NKp46⁺ cells during α -NK1.1 antibody depletion experiment. $n = 4$ per group. Unpaired two-tailed t -test. **j**, Quantification of NK1.1⁺CD200R^R NK cells in the spleen during α -NK1.1 antibody depletion experiment. $n = 4$ per group. Unpaired two-tailed t -test. Data are mean \pm s.e.m.



Extended Data Fig. 10. Control analyses of microbial regulation of NK cells and astrocytes.
a, Quantification of astrocytes from SPF ($n = 3$) or GF ($n = 5$) mice. Unpaired two-tailed t -test. **b**, Quantification of CD4⁺ T cells in SPF and GF mice. Splenic T cells: $n = 4$ per group; lamina propria T cells: $n = 3$ per group. Unpaired two-tailed t -test. **c**, IFN γ ⁺ NK cells in spleen and lamina propria of SPF and GF mice. $n = 5$ per group (spleen), $n = 6$ per group (lamina propria). Unpaired two-tailed t -test. **d**, Sorting schematic (left) and splenic cell numbers (right) from donors and recipients in NK cell adoptive transfer experiments. Quantification left-to-right: glow cytometry quantification of splenic IFN γ ⁺ NK cells from donor mice. $n = 5$ GF, $n = 8$ SPF WT, $n = 7$ SPF *Ifng*^{-/-} mice. Total number of NK cells from donor mice. $n = 6$ GF, $n = 8$ mice otherwise. Unpaired two-tailed t -test. Total number

of NK cells in recipient spleens: $n = 4$ mice per group. One-way ANOVA, Tukey's post-hoc test. **e**, Analysis by qPCR of 16S rRNA abundance as a function of two-week antibiotic treatment (ABX) and ABX treatment followed by faecal microbiota transplant (FMT) in *Ifng^{EYFP}* mice. $n = 6$ mice per group. Unpaired two-tailed *t*-test. **f**, Gating schematic for the meninges of *Ifng^{EYFP}* mice. **g**, FACS plots of IFN γ expression during three-week antibiotic depletion of commensal bacteria (ABX) or two-week ABX followed by 1-week reconstitution by faecal microbiota transplant (FMT) using *Ifng^{EYFP}* reporter mice. **h**, Analysis of NK cells in the spleen and lamina propria as a function of ABX and ABX + FMT treatment using *Ifng^{EYFP}* reporter mice. $n = 6$ mice for total NK cells ABX and ABX + FMT, $n = 10$ mice for vehicle meninges condition, $n = 5$ mice otherwise. Unpaired two-tailed *t*-test. **i**, Gating schematic of NK cell sorting from the spleen of *CAG^{Kaede}* mice. **j**, Analysis by qPCR of bacterial 16S rRNA abundance as a function of ABX and ABX + FMT in *CAG^{Kaede}* mice. $n = 9$ mice per group. Unpaired two-tailed *t*-test. Data are mean \pm s.e.m.

Supplementary Material

Refer to Web version on PubMed Central for supplementary material.

Acknowledgements

This work was supported by grants NS102807, ES02530, ES029136, AI126880 and AI149699 from the NIH; and RG4111A1 and JF2161-A-5 from the National Multiple Sclerosis Society (NMSS) (to F.J.Q.) F.J.Q. and A.P. received support from the International Progressive MS Alliance (PA-1604-08459); I.M.C. is supported by grants DP2AT009499 and R01AI130019 from the NIH, a Chan-Zuckerberg Initiative Ben Barres Early Career award and the Burroughs Wellcome fund; A.P. holds the T1 Canada Research Chair in MS and is funded by the Canada Institute of Health Research, the NMSS and the Canadian Foundation for Innovation; M.A.W. was supported by the NIH (1K99NS114111, F32NS101790), a training grant from the NIH and Dana-Farber Cancer Institute (T32CA207201), a travelling neuroscience fellowship from the Program in Interdisciplinary Neuroscience at the Brigham and Women's Hospital and the Women's Brain Initiative at the Brigham and Women's Hospital; C.G.-V. was supported by an Alfonso Martín Escudero Foundation postdoctoral fellowship and by a postdoctoral fellowship from the European Molecular Biology Organization (ALTF 610-2017); and C.M.P. was supported by a fellowship from the FAPESP BEPE (2019/13731-0). Sanger sequencing was carried out at the DNA Resource Core of Dana-Farber/Harvard Cancer Center (funded in part by NCI Cancer Center support grant 2P30CA006516-48). We thank T. Korn for sharing *Ifng^{EYFP}* reporter mice and U. von Andrian for sharing *CAG^{Kaede}* mice. We thank S. Boswell, M. Chatterjee, A. Ratner and the Harvard Medical School Single Cell Core for assistance with InDrop libraries; S. Garamszegi, T. Mason, E. LaRoche and the Broad Institute Genomics Platform for assistance with deep sequencing; R. Krishnan for assistance with flow cytometry studies, the use of the Harvard Digestive Disease Center (HDDC) core services, resources, technology and expertise; P. Hewson and G. Lipof for technical assistance; and all members of the Quintana laboratory for advice and discussions.

Data availability

All raw and processed deep sequencing data have been deposited into GEO under the SuperSeries accession number GSE144859. Source data are provided with this paper.

References

1. Linnerbauer M, Wheeler MA & Quintana FJ Astrocyte crosstalk in CNS inflammation. *Neuron* 108, 608–622 (2020). [PubMed: 32898475]
2. de Saint Basile G, Ménasché G & Fischer A Molecular mechanisms of biogenesis and exocytosis of cytotoxic granules. *Nat. Rev. Immunol* 10, 568–579 (2010). [PubMed: 20634814]
3. Aggarwal BB Signalling pathways of the TNF superfamily: a double-edged sword. *Nat. Rev. Immunol* 3, 745–756 (2003). [PubMed: 12949498]

4. Chao CC et al. Metabolic control of astrocyte pathogenic activity via cPLA2-MAVS. *Cell* 179, 1483–1498 (2019). [PubMed: 31813625]
5. Mächler P et al. In vivo evidence for a lactate gradient from astrocytes to neurons. *Cell Metab.* 23, 94–102 (2016). [PubMed: 26698914]
6. Nagai J et al. Hyperactivity with disrupted attention by activation of an astrocyte synaptogenic cue. *Cell* 177, 1280–1292 (2019). [PubMed: 31031006]
7. Allen NJ & Lyons DA Glia as architects of central nervous system formation and function. *Science* 362, 181–185 (2018). [PubMed: 30309945]
8. Sofroniew MV Astrocyte barriers to neurotoxic inflammation. *Nat. Rev. Neurosci* 16, 249–263 (2015). [PubMed: 25891508]
9. Alvarez JI et al. The Hedgehog pathway promotes blood-brain barrier integrity and CNS immune quiescence. *Science* 334, 1727–1731 (2011). [PubMed: 22144466]
10. Colonna M & Butovsky O Microglia function in the central nervous system during health and neurodegeneration. *Annu. Rev. Immunol* 35, 441–468 (2017). [PubMed: 28226226]
11. Liddelow SA & Barres BA Reactive astrocytes: production, function, and therapeutic potential. *Immunity* 46, 957–967 (2017). [PubMed: 28636962]
12. Prinz M, Jung S & Priller J Microglia biology: One century of evolving concepts. *Cell* 179, 292–311 (2019). [PubMed: 31585077]
13. Wheeler MA & Quintana FJ Regulation of astrocyte functions in multiple sclerosis. *Cold Spring Harb. Perspect. Med* 9, a029009 (2019). [PubMed: 29358321]
14. John Lin CC et al. Identification of diverse astrocyte populations and their malignant analogs. *Nat. Neurosci* 20, 396–405 (2017). [PubMed: 28166219]
15. Liddelow SA et al. Neurotoxic reactive astrocytes are induced by activated microglia. *Nature* 541, 481–487 (2017). [PubMed: 28099414]
16. Wheeler MA et al. MAFG-driven astrocytes promote CNS inflammation. *Nature* 578, 593–599 (2020). [PubMed: 32051591]
17. Ito M et al. Brain regulatory T cells suppress astrogliosis and potentiate neurological recovery. *Nature* 565, 246–250 (2019). [PubMed: 30602786]
18. Mayo L et al. IL-10-dependent Tr1 cells attenuate astrocyte activation and ameliorate chronic central nervous system inflammation. *Brain* 139, 1939–1957 (2016). [PubMed: 27246324]
19. Kipnis J Multifaceted interactions between adaptive immunity and the central nervous system. *Science* 353, 766–771 (2016). [PubMed: 27540163]
20. Rothhammer V et al. Type I interferons and microbial metabolites of tryptophan modulate astrocyte activity and central nervous system inflammation via the aryl hydrocarbon receptor. *Nat. Med* 22, 586–597 (2016). [PubMed: 27158906]
21. Erny D et al. Host microbiota constantly control maturation and function of microglia in the CNS. *Nat. Neurosci* 18, 965–977 (2015). [PubMed: 26030851]
22. Rothhammer V et al. Microglial control of astrocytes in response to microbial metabolites. *Nature* 557, 724–728 (2018). [PubMed: 29769726]
23. Sampson TR et al. Gut microbiota regulate motor deficits and neuroinflammation in a model of Parkinson's disease. *Cell* 167, 1469–1480 (2016). [PubMed: 27912057]
24. Thion MS et al. Microbiome influences prenatal and adult microglia in a sex-specific manner. *Cell* 172, 500–516 (2018). [PubMed: 29275859]
25. Wheeler MA et al. Environmental control of astrocyte pathogenic activities in CNS inflammation. *Cell* 176, 581–596 (2019). [PubMed: 30661753]
26. Pender MP, McCombe PA, Yoong G & Nguyen KB Apoptosis of $\alpha\beta$ T lymphocytes in the nervous system in experimental autoimmune encephalomyelitis: its possible implications for recovery and acquired tolerance. *J. Autoimmun* 5, 401–410 (1992). [PubMed: 1384526]
27. Schmied M et al. Apoptosis of T lymphocytes in experimental autoimmune encephalomyelitis. Evidence for programmed cell death as a mechanism to control inflammation in the brain. *Am. J. Pathol* 143, 446–452 (1993). [PubMed: 8342595]

28. Zeine R & Owens T Loss rather than downregulation of CD4⁺ T cells as a mechanism for remission from experimental allergic encephalomyelitis. *J. Neuroimmunol* 44, 193–198 (1993). [PubMed: 8099362]
29. Lee Y et al. Induction and molecular signature of pathogenic T_H17 cells. *Nat. Immunol* 13, 991–999 (2012). [PubMed: 22961052]
30. Ferber IA et al. Mice with a disrupted IFN-gamma gene are susceptible to the induction of experimental autoimmune encephalomyelitis (EAE). *J. Immunol* 156, 5–7 (1996). [PubMed: 8598493]
31. Wilson NS, Dixit V & Ashkenazi A Death receptor signal transducers: nodes of coordination in immune signaling networks. *Nat. Immunol* 10, 348–355 (2009). [PubMed: 19295631]
32. Colonna M Innate lymphoid cells: diversity, plasticity, and unique functions in immunity. *Immunity* 48, 1104–1117 (2018). [PubMed: 29924976]
33. Filiano AJ et al. Unexpected role of interferon- γ in regulating neuronal connectivity and social behaviour. *Nature* 535, 425–429 (2016). [PubMed: 27409813]
34. Ganal SC et al. Priming of natural killer cells by nonmucosal mononuclear phagocytes requires instructive signals from commensal microbiota. *Immunity* 37, 171–186 (2012). [PubMed: 22749822]
35. Thiemann S et al. Enhancement of IFN γ production by distinct commensals ameliorates salmonella-induced disease. *Cell Host Microbe* 21, 682–694 (2017). [PubMed: 28618267]
36. Tomura M et al. Monitoring cellular movement in vivo with photoconvertible fluorescence protein “Kaede” transgenic mice. *Proc. Natl Acad. Sci. USA* 105, 10871–10876 (2008). [PubMed: 18663225]
37. Mayo L et al. Regulation of astrocyte activation by glycolipids drives chronic CNS inflammation. *Nat. Med* 20, 1147–1156 (2014). [PubMed: 25216636]
38. Bai Z et al. Cerebrospinal fluid and blood cytokines as biomarkers for multiple sclerosis: a systematic review and meta-analysis of 226 studies with 13,526 multiple sclerosis patients. *Front. Neurosci* 13, 1026 (2019). [PubMed: 31636528]
39. Foo LC et al. Development of a method for the purification and culture of rodent astrocytes. *Neuron* 71, 799–811 (2011). [PubMed: 21903074]
40. Baruch K et al. Aging-induced type I interferon response at the choroid plexus negatively affects brain function. *Science* 346, 89–93 (2014). [PubMed: 25147279]
41. Gross CC et al. Regulatory functions of natural killer cells in multiple sclerosis. *Front. Immunol* 7, 606 (2016). [PubMed: 28066417]
42. Gross CC et al. Impaired NK-mediated regulation of T cell activity in multiple sclerosis is reconstituted by IL-2 receptor modulation. *Proc. Natl Acad. Sci. USA* 113, E2973–E2982 (2016). [PubMed: 27162345]
43. Cella M, Otero K & Colonna M Expansion of human NK-22 cells with IL-7, IL-2, and IL-1 β reveals intrinsic functional plasticity. *Proc. Natl Acad. Sci. USA* 107, 10961–10966 (2010). [PubMed: 20534450]
44. Sun JC, Beilke JN & Lanier LL Adaptive immune features of natural killer cells. *Nature* 457, 557–561 (2009). [PubMed: 19136945]
45. Ascherio A, Munger KL & Lünemann JD The initiation and prevention of multiple sclerosis. *Nat. Rev. Neurol* 8, 602–612 (2012). [PubMed: 23045241]
46. Rojas OL et al. Recirculating intestinal IgA-producing cells regulate neuroinflammation via IL-10. *Cell* 177, 492–493 (2019). [PubMed: 30951673]
47. Kadowaki A & Quintana FJ The gut-CNS axis in multiple sclerosis. *Trends Neurosci.* 43, 622–634 (2020). [PubMed: 32650957]
48. Korn T & Kallies A T cell responses in the central nervous system. *Nat. Rev. Immunol* 17, 179–194 (2017). [PubMed: 28138136]
49. Codarri L et al. ROR γ t drives production of the cytokine GM-CSF in helper T cells, which is essential for the effector phase of autoimmune neuroinflammation. *Nat. Immunol* 12, 560–567 (2011). [PubMed: 21516112]

50. El-Behi M et al. The encephalitogenicity of T_H17 cells is dependent on IL-1- and IL-23-induced production of the cytokine GM-CSF. *Nat. Immunol* 12, 568–575 (2011). [PubMed: 21516111]
51. Khakh BS & Deneen B The emerging nature of astrocyte diversity. *Annu. Rev. Neurosci* 42, 187–207 (2019). [PubMed: 31283899]
52. Buffington SA et al. Microbial reconstitution reverses maternal diet-induced social and synaptic deficits in offspring. *Cell* 165, 1762–1775 (2016). [PubMed: 27315483]
53. Chu C et al. The microbiota regulate neuronal function and fear extinction learning. *Nature* 574, 543–548 (2019). [PubMed: 31645720]
54. Rothhammer V et al. Sphingosine 1-phosphate receptor modulation suppresses pathogenic astrocyte activation and chronic progressive CNS inflammation. *Proc. Natl Acad. Sci. USA* 114, 2012–2017 (2017). [PubMed: 28167760]
55. Sanjana NE, Shalem O & Zhang F Improved vectors and genome-wide libraries for CRISPR screening. *Nat. Methods* 11, 783–784 (2014). [PubMed: 25075903]
56. Chen S et al. Genome-wide CRISPR screen in a mouse model of tumor growth and metastasis. *Cell* 160, 1246–1260 (2015). [PubMed: 25748654]
57. Lee Y, Messing A, Su M & Brenner M GFAP promoter elements required for region-specific and astrocyte-specific expression. *Glia* 56, 481–493 (2008). [PubMed: 18240313]
58. Wang T et al. Gene essentiality profiling reveals gene networks and synthetic lethal interactions with oncogenic Ras. *Cell* 168, 890–903 (2017). [PubMed: 28162770]
59. Foo LC Purification of rat and mouse astrocytes by immunopanning. *Cold Spring Harb. Protoc* 2013, pdb.prot074211 (2013).
60. Beaudoin GM III et al. Culturing pyramidal neurons from the early postnatal mouse hippocampus and cortex. *Nat. Protoc* 7, 1741–1754 (2012). [PubMed: 22936216]
61. Yates A et al. Ensembl 2016. *Nucleic Acids Res.* 44, D710–D716 (2016). [PubMed: 26687719]
62. Ovcharenko I et al. Mulan: multiple-sequence local alignment and visualization for studying function and evolution. *Genome Res.* 15, 184–194 (2005). [PubMed: 15590941]
63. Untergasser A et al. Primer3—new capabilities and interfaces. *Nucleic Acids Res.* 40, e115 (2012). [PubMed: 22730293]
64. Keren-Shaul H et al. A unique microglia type associated with restricting development of Alzheimer’s disease. *Cell* 169, 1276–1290 (2017). [PubMed: 28602351]
65. Louveau A et al. Structural and functional features of central nervous system lymphatic vessels. *Nature* 523, 337–341 (2015). [PubMed: 26030524]
66. Xu H et al. Transcriptional atlas of intestinal immune cells reveals that neuropeptide α -CGRP modulates group 2 innate lymphoid cell responses. *Immunity* 51, 696–708 (2019). [PubMed: 31618654]
67. Kim RY et al. Astrocyte CCL2 sustains immune cell infiltration in chronic experimental autoimmune encephalomyelitis. *J. Neuroimmunol* 274, 53–61 (2014). [PubMed: 25005117]
68. Schläger C et al. Effector T-cell trafficking between the leptomeninges and the cerebrospinal fluid. *Nature* 530, 349–353 (2016). [PubMed: 26863192]
69. Kolev M et al. Diapedesis-induced integrin signaling via LFA-1 facilitates tissue immunity by inducing intrinsic complement C3 expression in immune cells. *Immunity* 52, 513–527 (2020). [PubMed: 32187519]
70. Polman CH et al. Diagnostic criteria for multiple sclerosis: 2010 revisions to the McDonald criteria. *Ann. Neurol* 69, 292–302 (2011). [PubMed: 21387374]
71. Klein AM et al. Droplet barcoding for single-cell transcriptomics applied to embryonic stem cells. *Cell* 161, 1187–1201 (2015). [PubMed: 26000487]
72. Zhang X et al. Comparative analysis of droplet-based ultra-high-throughput single-cell RNA-seq systems. *Mol. Cell* 73, 130–142 (2019). [PubMed: 30472192]
73. Langmead B & Salzberg SL Fast gapped-read alignment with Bowtie 2. *Nat. Methods* 9, 357–359 (2012). [PubMed: 22388286]
74. Butler A, Hoffman P, Smibert P, Papalexis E & Satija R Integrating single-cell transcriptomic data across different conditions, technologies, and species. *Nat. Biotechnol* 36, 411–420 (2018). [PubMed: 29608179]

75. Stuart T et al. Comprehensive integration of single-cell data. *Cell* 177, 1888–1902 (2019). [PubMed: 31178118]
76. Finak G et al. MAST: a flexible statistical framework for assessing transcriptional changes and characterizing heterogeneity in single-cell RNA sequencing data. *Genome Biol.* 16, 278 (2015). [PubMed: 26653891]
77. Macosko EZ et al. Highly parallel genome-wide expression profiling of individual cells using nanoliter droplets. *Cell* 161, 1202–1214 (2015). [PubMed: 26000488]
78. Becht E et al. Dimensionality reduction for visualizing single-cell data using UMAP. *Nat. Biotechnol* 37, 38–44 (2019).
79. van der Maaten L & Hinton G Visualizing data using t-SNE. *J. Mach. Learn. Res* 9, 2579–2605 (2008).
80. Trombetta JJ et al. Preparation of single-cell RNA-seq libraries for next generation sequencing. *Curr. Protoc. Mol. Biol* 107, 4.22.1–4.22.17 (2014). [PubMed: 24984854]
81. Bray NL, Pimentel H, Melsted P & Pachter L Near-optimal probabilistic RNA-seq quantification. *Nat. Biotechnol* 34, 525–527 (2016). [PubMed: 27043002]
82. Patro R, Duggal G, Love MI, Irizarry RA & Kingsford C Salmon provides fast and bias-aware quantification of transcript expression. *Nat. Methods* 14, 417–419 (2017). [PubMed: 28263959]
83. Zhu A, Ibrahim JG & Love MI Heavy-tailed prior distributions for sequence count data: removing the noise and preserving large differences. *Bioinformatics* 35, 2084–2092 (2019). [PubMed: 30395178]
84. Subramanian A et al. Gene set enrichment analysis: a knowledge-based approach for interpreting genome-wide expression profiles. *Proc. Natl Acad. Sci. USA* 102, 15545–15550 (2005). [PubMed: 16199517]
85. Mootha VK et al. PGC-1 α -responsive genes involved in oxidative phosphorylation are coordinately downregulated in human diabetes. *Nat. Genet* 34, 267–273 (2003). [PubMed: 12808457]
86. Chen EY et al. Enrichr: interactive and collaborative HTML5 gene list enrichment analysis tool. *BMC Bioinformatics* 14, 128 (2013). [PubMed: 23586463]
87. Kuleshov MV et al. Enrichr: a comprehensive gene set enrichment analysis web server 2016 update. *Nucleic Acids Res.* 44, W90–W97 (2016). [PubMed: 27141961]
88. Mi H, Muruganujan A, Ebert D, Huang X & Thomas PD PANTHER version 14: more genomes, a new PANTHER GO-slim and improvements in enrichment analysis tools. *Nucleic Acids Res.* 47, D419–D426 (2019). [PubMed: 30407594]

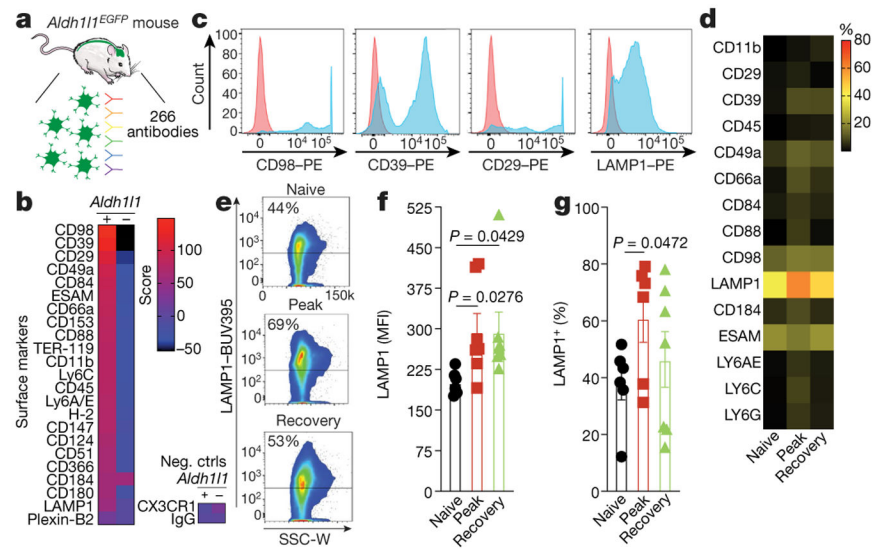


Fig. 1 | Profiling astrocyte surface markers in EAE.

a, Analysis of CNS samples from naive *Aldh11^{EGFP}* mice ($n = 32$). **b**, Top 42 surface markers and negative controls (neg. ctrls) expressed by astrocytes (*Aldh11⁺*) versus non-astrocytes (*Aldh11⁻*). **c**, Histograms depicting staining of surface-molecule antibodies (blue) and isotype control (red) gated on astrocytes (*Aldh11⁺*). **d**, Fluorescence-activated cell sorting (FACS) analysis of tdTomato⁺CX3CR1⁻ astrocytes from the spinal cord of naive and EAE peak or EAE recovery *Aldh11^{creERT2}tdTomato* mice ($n = 7$ for the EAE recovery group (except $n = 6$ for CD29); $n = 6$ mice otherwise). **e**, FACS plots of LAMP1⁺ astrocytes during EAE. **f**, **g**, LAMP1 expression in astrocytes from the spinal cord, measured as mean fluorescence intensity (MFI) (**f**) and as a percentage (**g**) from the screen in **d** ($n = 6$ mice for the naive group in **f** and the EAE peak group in **g**; $n = 7$ mice otherwise). Unpaired two-tailed *t*-test. Data are mean \pm s.e.m. (**f**, **g**).

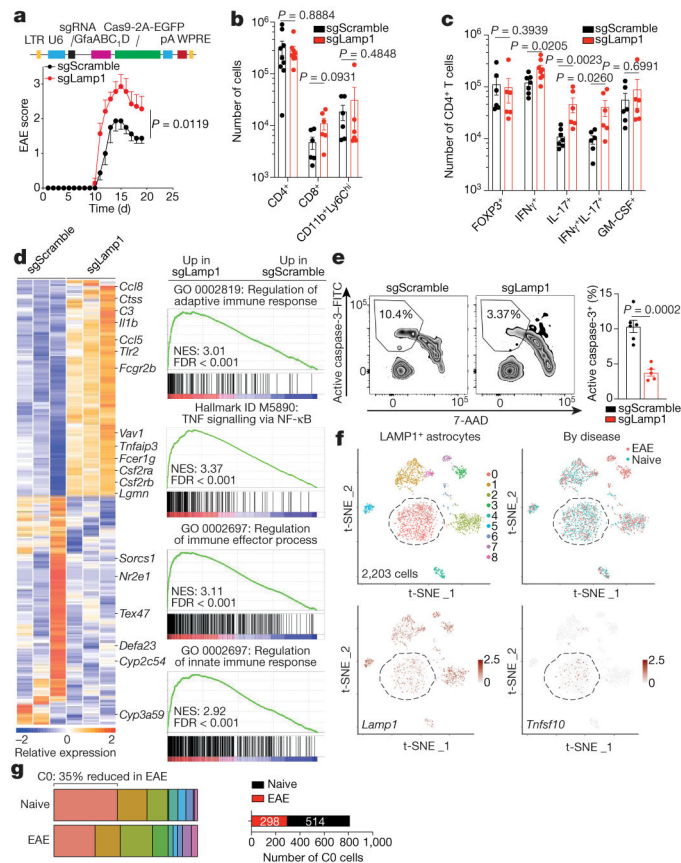


Fig. 2 | LAMP1⁺ astrocytes limit CNS inflammation and express TRAIL.

a, Top, schematic of lentivirus vector. Bottom, EAE curves in mice treated with sgRNA against *Lamp1* (sgLamp1) or control scramble sgRNA (sgScramble) ($n = 19$ sgScramble; $n = 15$ sgLamp1 mice). Experiment repeated three times. Two-way repeated measures analysis of variance (ANOVA). **b**, Quantification of immune cells in sgScramble- or sgLamp1-transduced mice ($n = 9$ sgScramble CD4⁺; $n = 8$ sgLamp1 CD4⁺; $n = 6$ mice otherwise). Two-tailed Mann–Whitney test. **c**, Quantification of the CD4⁺ T cell subset in sgScramble- or sgLamp1-transduced mice ($n = 8$ IFN γ ⁺; $n = 7$ sgScramble IFN γ ⁺IL-17⁺; $n = 6$ mice otherwise). Two-tailed Mann–Whitney test. **d**, Left, differential gene expression determined by bulk RNA-seq in sgScramble- or sgLamp1-transduced mice. Right, gene set enrichment analysis (GSEA) comparing sgScramble- and sgLamp1-transduced mice (day 19 after EAE induction; $n = 3$ mice per group). Gene Ontology (GO) terms are shown. FDR, false discovery rate; NES, normalized enrichment score. **e**, FACS analysis of activation of caspase-3 in CNS CD4⁺ T cells ($n = 6$ sgScramble; $n = 5$ sgLamp1 mice). Unpaired two-tailed *t*-test. **f**, Top, *t*-distributed stochastic neighbour embedding (t-SNE) plots of LAMP1⁺ astrocytes from naive or EAE *Aldh111^{creERT2tdTomato}* mice (day 17 after EAE induction; $n = 3$ mice per group) analysed by scRNA-seq. Bottom, t-SNE plots of *Lamp1* and *Tnfsf10*. **g**, Left, distribution of scRNA-seq clusters by condition. Right, number of cluster 0 (C0) cells ($n = 812$ cells). Data are mean \pm s.e.m. (**a–c**, **e**).

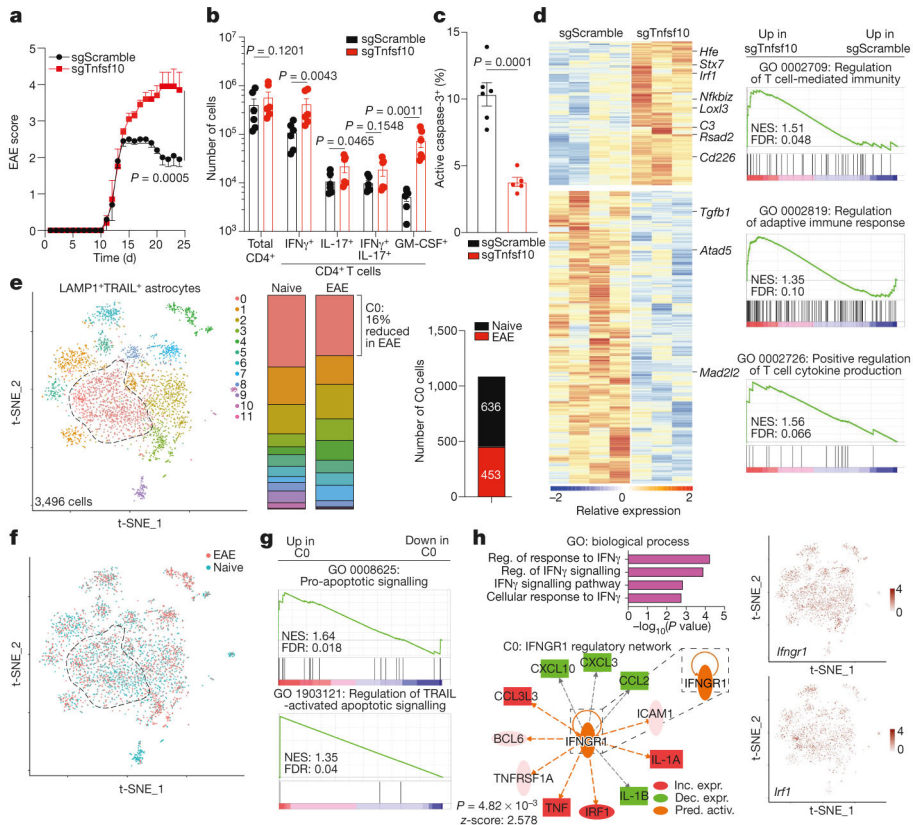


Fig. 3 | TRAIL⁺ astrocytes limit EAE development.

a, EAE curves in sgScramble ($n = 24$) and sgTnfsf10 ($n = 25$) mice. Experiment repeated three times. Two-way repeated measures ANOVA. **b**, Quantification of T cell subsets (day 24 after EAE induction; $n = 6$ mice per group). One-tailed Mann–Whitney test. **c**, Activation of caspase-3 in CNS CD4⁺ T cells ($n = 6$ sgScramble; $n = 5$ sgTnfsf10 mice). Unpaired two-tailed t -test. **d**, Left, differential gene expression determined by bulk RNA-seq in astrocytes isolated from sgScramble ($n = 4$) or sgTnfsf10 ($n = 3$)-transduced mice (left) at 24 days after EAE induction. Right, GSEA comparing sgScramble- and sgTnfsf10-transduced mice. **e**, **f**, Left, t-SNE plots of LAMP1⁺TRAIL⁺ astrocytes from naive or EAE *Aldh111*^{creERT2tdTomato} mice (day 17 after EAE induction; $n = 3$ mice per group) analysed by scRNA-seq. **e**, Right, number of cluster 0 cells ($n = 1,089$ cells). **g**, GSEA of C0 astrocytes. **h**, Top left, GO analysis of differentially upregulated pathways in C0 astrocytes. Reg., regulation. Bottom left, predicted upstream regulation of the C0 transcriptional signature using Ingenuity Pathway Analysis (Qiagen). Inc. expr., increased expression; dec. expr., decreased expression; pred. activ., predicted activation. Right, t-SNE plots of *Ifngr1* and *Irf1*. Data are mean \pm s.e.m. (**a–c**).

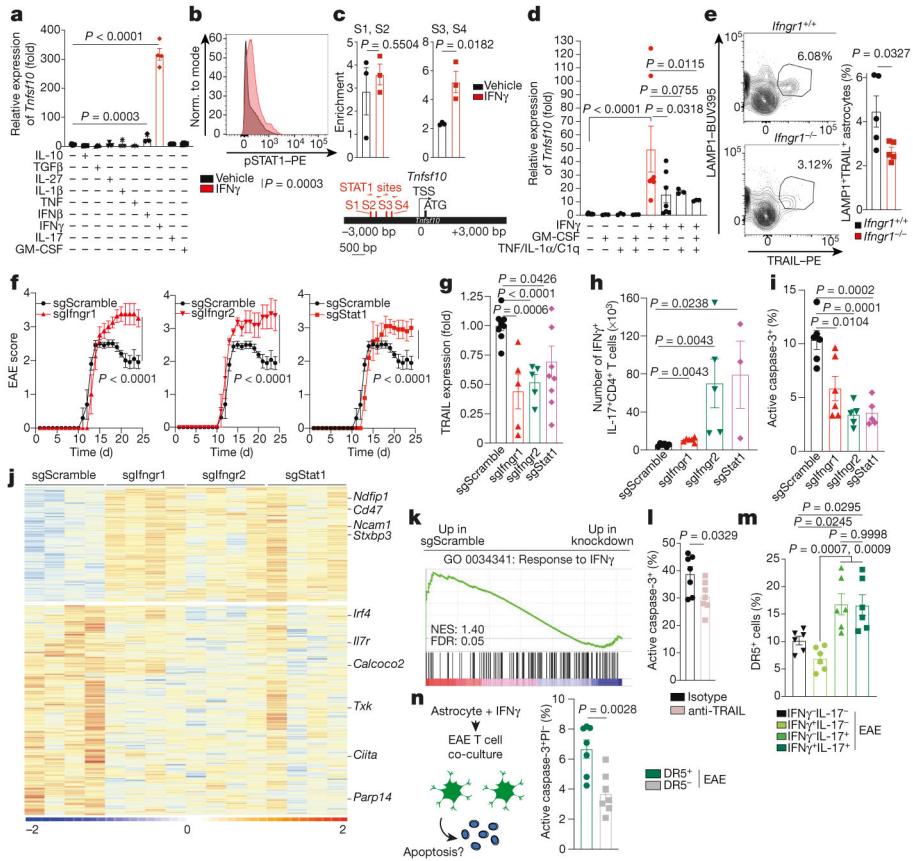


Fig. 4 | IFN γ induces TRAIL expression in astrocytes.

a, Quantitative PCR (qPCR) of *Tnfsf10* expression in mouse primary astrocytes ($n = 11$ vehicle; $n = 3$ IL-1 β ; $n = 3$ TNF; $n = 3$ IFN β ; $n = 4$ biological replicates otherwise). Unpaired two-tailed *t*-test. **b**, Levels of pSTAT1 in mouse primary astrocytes after 60-min treatment with IFN γ or vehicle ($n = 4$ biological replicates per condition). Experiment repeated three times. Unpaired two-tailed *t*-test. **c**, Bottom, STAT1-binding motifs (STAT1 sites 1–4; S1–S4) in the *Tnfsf10* promoter. Top, STAT1 chromatin immunoprecipitation (ChIP)-qPCR after IFN γ or vehicle treatment. $n = 3$ per condition. Unpaired two-tailed *t*-test. **d**, qPCR of *Tnfsf10* expression in mouse primary astrocytes ($n = 7$ vehicle, IFN γ , IFN γ + GM-CSF; $n = 3$ mice otherwise). Welch’s two-tailed *t*-test, *In*-normalized data. **e**, FACS analysis of LAMP1⁺TRAIL⁺ astrocytes (day 28 after EAE induction; $n = 5$ per group). Unpaired two-tailed *t*-test. **f**, EAE curves ($n = 24$ sgScramble; $n = 18$ sgIfngr1; $n = 14$ sgIfngr2; $n = 12$ sgStat1 mice). Experiment repeated three times. Two-way repeated measures ANOVA. **g**, TRAIL expression in astrocytes of knockdown mice ($n = 9$ sgScramble; $n = 5$ sgIfngr1; $n = 5$ sgIfngr2; $n = 9$ sgStat1 mice). Unpaired two-tailed *t*-test. **h**, FACS analysis of CNS IFN γ ⁺IL-17⁺CD4⁺ T cells in knockdown mice ($n = 6$ sgScramble, $n = 6$ sgIfngr1, $n = 5$ sgIfngr2, $n = 3$ sgStat1 mice). Two-tailed Mann–Whitney test. **i**, Activation of caspase-3 in CNS CD4⁺T cells ($n = 6$ sgScramble, sgIfngr1; $n = 5$ mice otherwise). Unpaired two-tailed *t*-test. **j**, **k**, Heat map (**j**) and GSEA (**k**) of astrocyte gene expression (day 24 after EAE induction; $n = 4$ mice per group). **l**, Activation of caspase-3 in CD4⁺T cells co-cultured with astrocytes and anti-TRAIL blocking antibody ($n = 7$

biological replicates) per condition. Unpaired two-tailed *t*-test. **m**, Expression of DR5 in CD4⁺ T cells in peak EAE mice (day 18 after EAE induction; *n* = 6 mice per group). One-way ANOVA, Tukey's post-hoc test. **n**, Schematic (left) and quantification (right) of active caspase-3 expression in DR5⁺ and DR5⁻ CD4⁺ T cells isolated from peak EAE mice (day 18 after EAE induction), co-cultured with IFN γ -pre-treated astrocytes (*n* = 7 biological replicates per group) PI, propidium iodide. Unpaired two-tailed *t*-test. Data are mean \pm s.e.m. (**a**, **c**, **d-i**, **l-n**).

Author Manuscript

Author Manuscript

Author Manuscript

Author Manuscript

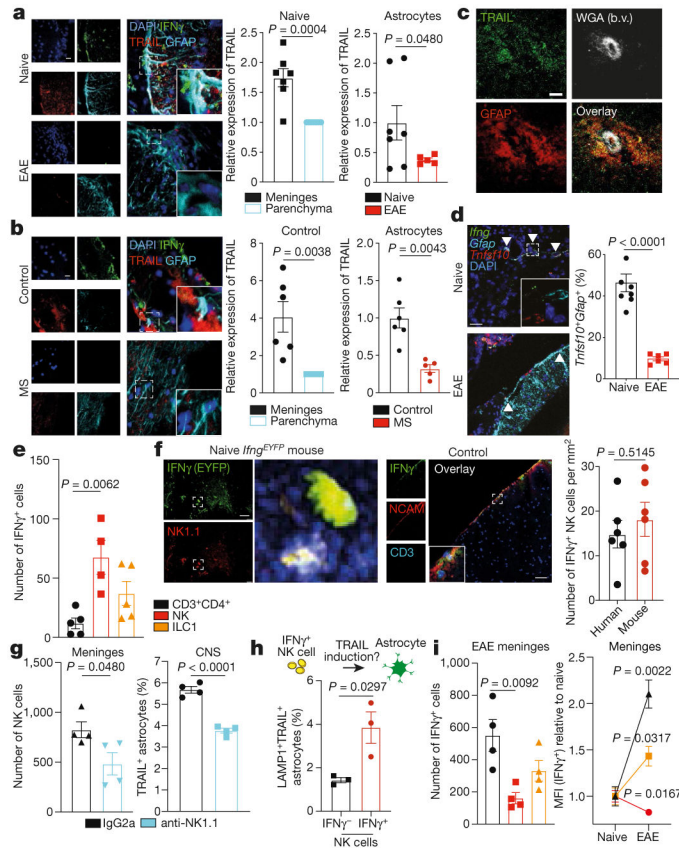


Fig. 5 | Meningeal IFN γ ⁺ NK cells promote homeostatic astrocyte TRAIL expression.
a, Left, immunostaining of spinal cord sections from naive and EAE mice ($n = 7$ sections (naive); $n = 5$ sections (EAE); $n = 3$ mice per group). Right, quantification of TRAIL expression normalized to control or parenchyma within images. Unpaired two-tailed t -test (left) and Kolmogorov–Smirnov test (right). Scale bar, 20 μm . **b**, Left, immunostaining of meninges from healthy control individuals (control) and from patients with MS ($n = 6$ sections (control); $n = 5$ sections (MS); $n = 3$ patients per group). Right, TRAIL expression quantified as in **a**. Unpaired two-tailed t -test (left) and Kolmogorov–Smirnov test (right). Scale bar, 20 μm . **c**, Immunostaining of TRAIL⁺ astrocytes in mouse CNS after peripheral intravenous injection of fluorescent WGA. b.v., blood vessel. Experiment repeated twice. Scale bar, 15 μm . **d**, RNAscope analysis of mouse spinal cord ($n = 8$ images (naive); $n = 6$ images (EAE)). Unpaired two-tailed t -test. Experiment repeated three times. Scale bar, 15 μm . **e**, IFN γ expression determined by flow cytometry in meninges from naive mice. NK cells, NK1.1⁺CD200R⁻; type-1 innate lymphoid cells (ILC1), NK1.1⁺CD200R⁺ ($n = 4$ mice (NK); $n = 5$ mice otherwise). One-way ANOVA, Tukey’s post-hoc test. **f**, Quantification of IFN γ ⁺ NK cells in meninges from *Ifng*^{EYFP} mice (left) or in meninges from healthy control individuals (right) ($n = 6$ mice; $n = 6$ individuals). Unpaired two-tailed t -test. Scale bars, 100 μm . **g**, FACS analysis of meningeal NK cells (left) and TRAIL⁺ astrocytes (right) 72 h after treatment with anti-NK1.1 or isotype control antibody ($n = 4$ mice per group). Unpaired two-tailed t -test. **h**, FACS analysis of LAMP1⁺TRAIL⁺ astrocytes co-cultured with IFN γ ⁺ or IFN γ ⁻ NK cells from *Ifng*^{EYFP} mice ($n = 3$ per group). Unpaired two-tailed t -test. **i**, FACS

analysis of IFN γ ⁺ cells (left) and MFI (right) in meninges from naive and EAE (day 22 after EAE induction) mice. Left: $n = 4$ mice per group. One-way ANOVA, Tukey's post-hoc test. Right: $n = 3$ naive; $n = 5$ EAE mice. Unpaired two-tailed t -test per cell type by condition. Data are mean \pm s.e.m. (**a**, **b**, **d**, **e-i**).

Author Manuscript

Author Manuscript

Author Manuscript

Author Manuscript

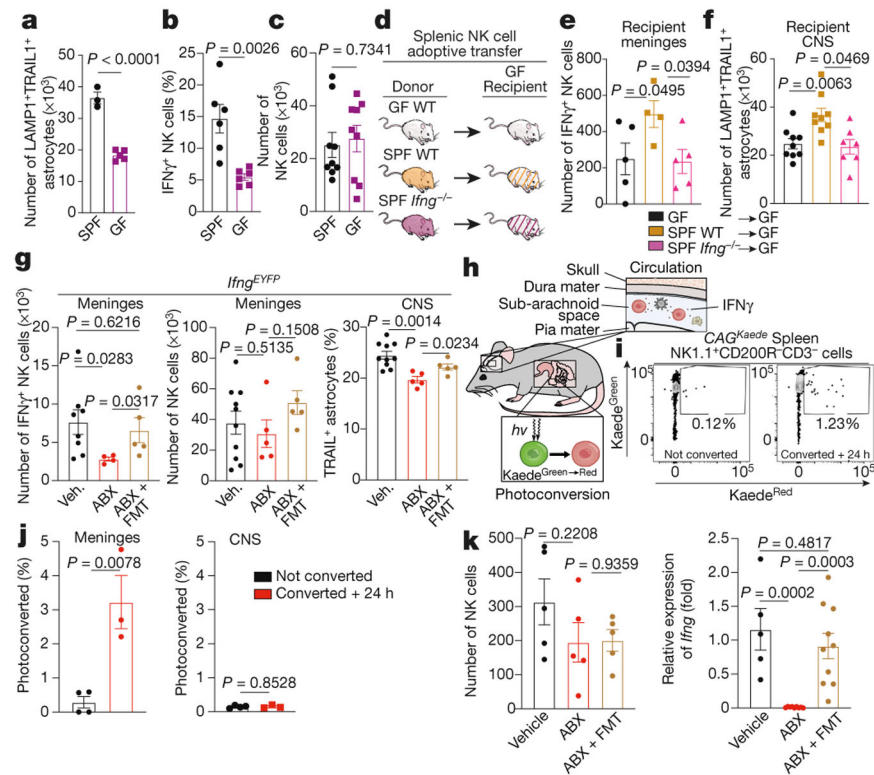


Fig. 6 | The microbiome modulates LAMP1⁺TRAIL⁺ astrocytes through meningeal IFN γ ⁺ NK cells.

a–c, FACS analysis of LAMP1⁺TRAIL⁺ astrocytes (**a**), meningeal IFN γ ⁺NK (NK1.1⁺CD200R⁻) cells (**b**) and meningeal NK cells (**c**) in SPF and germ-free (GF) mice ($n = 3$ SPF mice; $n = 5$ GF mice (**a**); $n = 6$ mice per group (**b**); $n = 9$ mice per group (**c**)). Unpaired two-tailed t -test. **d**, Schematic of adoptive transfer experiment. WT, wild type. **e, f**, FACS analysis of meningeal IFN γ ⁺ NK cells (**e**) and LAMP1⁺TRAIL⁺ astrocytes (**f**) in mice receiving 1×10^6 NK cells (**e**: $n = 4$ SPF wild type; $n = 5$ mice otherwise; one-way ANOVA, Fisher's test; **f**: $n = 10$ SPF wild type; $n = 9$ *Ifng*^{-/-} mice; Kolmogorov–Smirnov two-tailed test). *Ifng*^{-/-} data are log-normalized in **f**. **g**, FACS analysis of IFN γ ⁺NK1.1⁺CD200R⁻ cells in the meninges (left), total NK1.1⁺CD200R⁻ cells in the meninges (middle) and TRAIL⁺ astrocytes in the CNS (right) of mice treated as indicated (left: $n = 8$ vehicle, $n = 4$ ABX, $n = 5$ ABX + FMT mice; middle: $n = 10$ vehicle, $n = 5$ mice otherwise; right: $n = 10$ vehicle, $n = 5$ mice otherwise). Two-tailed Mann–Whitney test (left, middle); unpaired two-tailed t -test (right). **h**, Schematic of Kaede photoconversion experiment. **i**, Representative analysis of splenic NK1.1⁺CD200R⁻CD3⁻ cells after photoconversion in the small intestine. Conv, converted. **j**, Quantification of NK cells in meninges and CNS parenchyma after photoconversion in the small intestine ($n = 4$ mice not converted; $n = 3$ mice converted + 24 h). Unpaired two-tailed t -test. **k**, Quantification of splenic NK cells (left) and *Ifng* expression in splenic NK cells (right) in mice after small intestine photoconversion and indicated treatments (left: $n = 5$ mice per group; right: $n = 5$ vehicle; $n = 9$ ABX; $n = 10$ ABX + FMT mice). Unpaired two-tailed t -test. Data are mean \pm s.e.m. (**a–c**, **e–g**, **i–k**).